POLITECNICO DI TORINO

Politecnico di Torino

MASTER DEGREE IN ENERGY AND NUCLEAR ENGINEERING

A.Y. 2023/2024

EXERGO-ECONOMIC ANALYSIS AND INTEGRATION OF ENERGY STORAGE SYSTEMS BASED ON TRANSCRITICAL CO_2

Advisors:

Prof. Elisa GUELPA

Prof. Vittorio VERDA

Student:

Corinna FLEMATTI

Co-Advisors:

Prof. Ricardo CHACARTEGUI RAMIREZ

JULY 2024

Abstract

Energy storage systems are essential for the deployment of renewable energy at large scale and the use of CO_2 as working fluid has experienced a significant boost in recent years due to its unique thermo-physical properties. This thesis presents a conceptual large scale thermoelectrical energy storage system based on a reversible heat pump that works with CO_2 in transcritical conditions. An exergo-economic analysis of the base close system is performed to determine the thermodynamic and economic feasibility of this kind of technology. Then, different possible integration scenarios for the base case are proposed and analysed; an open cycle that stores CO_2 and performs a geological injection of it; low and high temperature storage integrations to maximize the performance of the base case.

Table of contents

1. Introduction 10
2. Electrothermal energy storage using transcritical CO2 cycles 12
   2.1 Transcritical or supercritical cycle 12
   2.2 Reversible heat pump 14
3. Physical structure of the system 16
4. Productive structure of the system 20
5. Aspen Hysys® modelling 21
6. Energy analysis 24
7. Exergo-economic analysis 28
   7.1 Exergy cost analysis 31
   7.2 Cost of components 36
      7.2.1 Compressor 40
      7.2.2 Pump 41
      7.2.3 Turbine 43
      7.2.4 Heat exchangers 45
   7.3 Techno Economic-Analysis 51
   7.4 Financial Analysis 52
   7.5 Economic Analysis 55
8. Economic Indicators 61
   8.1 Total Capital Expenditure of the plant 61
   8.2 Total Operational Cost of the plant 62
   8.3 Net Present Value 62
   8.4 Other economic indicators 64
9. Sensitivity Analysis 66
10. 2023 scenario analysis 68
11. Integration scenarios for the reference system 71
   11.1 Open cycle system 71
      11.1.1 Aspen Hysys® modelling 73
   11.2 Low temperature integration 77
      11.2.1 Refrigerants for latent heat exchange 79
      11.2.2 Absorption chiller 84
   11.3 High temperature integration 89
      11.3.1 Cascade heat pump 90

12. Conclusions......94
13. References......95

List of Tables

Table 1. Incidence matrix of the considered system 18
Table 2. Productive structure of the whole system 20
Table 3. Property methods used for each fluid 21
Table 4. Main assumptions, inputs and hypothesis on the modelling of the charge cycle for the base case 22
Table 5. Main assumptions, inputs and hypothesis on the modelling of the discharge cycle for the base case 23
Table 6. Thermodynamic state of the mass streams for the reference system 27
Table 7. Exergy vector 29
Table 8. Irreversibility vector 30
Table 9. Cost matrix of the system 35
Table 10. Vector of external assessments 35
Table 11. Exergy cost vector 36
Table 12. Unit exergy cost vector 36
Table 13. Cost exponent for each component [24] 38
Table 14. Corrected factor related to temperature and material for centrifugal compressor 41
Table 15. Corrected factor related to temperature and material for reciprocating pump 43
Table 16. Corrected factor related to temperature and material for turbine 44
Table 17. Main results for the heat exchangers 47
Table 18. Pressure factor for plate-type heat exchanger 47
Table 19. Material factor for plate-type heat exchanger 47
Table 20. Percentages applied on the BEC 51
Table 21. Results from the BEC to the TASC 52
Table 22. Summary of the parameters used for the financial analysis 54
Table 23. Present value estimated on the 30 years of life of the plant 54
Table 24. Cost rates of components vector 56
Table 25. Resources cost vector 59
Table 26. Cost rates vector 60
Table 27. Cost vector 60
Table 28. Unit cost vector 60
Table 29. Values of the economic indicators 65
Table 30. Sensitivity analysis to the retail price 66

Table 31. Sensitivity analysis to the availability 66
Table 32. Sensitivity analysis to the electricity cost 66
Table 33. Comparison between electricity cost and CEPCI 68
Table 35. Main assumptions, inputs and hypothesis on the modelling of the open charge cycle 75
Table 36. Main assumptions, inputs and hypothesis on the modelling of the open discharge cycle ... 76
Table 37. Thermodynamic state of the mass streams for the open cycle 77
Table 38. First generation of refrigerants and their properties 79
Table 39. Second generation of refrigerants and their properties 80
Table 40. Third generation of refrigerants and their properties 80
Table 41. Natural refrigerants and their properties 81
Table 42. Results of the mass flow rate using R-290 for the charge and discharge cycle 81
Table 43. Results of the mass flow rate using R-717 for the charge and discharge cycle 83
Table 44. Main assumptions, inputs and hypothesis on the modelling of the absorption chiller cycle 88
Table 45. Thermodynamic state of the mass streams for the absorption chiller cycle 88
Table 46. Main assumptions, inputs and hypothesis on the modelling of the cascade heat pump 92
Table 47. Thermodynamic state of the mass streams for the system with the cascade heat pump 93

List of Figures

Reversible heat pump energy storage system with well-integrated temperature profile 14
Scheme of the reference system..... 16
Scheme of the reference system highlighting the control volume 17
Exergy destroyed percentages associated at each component..... 30
Values of CEPCI for each month of the year 2022 39
Off-peak hours electricity cost for Spain in 2022 58
Peak hours electricity cost for Spain in 2022..... 58
Net Present Value trend over the lifetime of the plant for the year 2022 63
Spider Diagram resulting from the sensitivity analysis..... 67
Off-peak hours electricity cost for Spain in 2023 69
Peak hours electricity cost for Spain in 2023..... 69
Net Present Value trend over the lifetime of the plant for the year 2023 70
Reversible heat pump energy storage system with well-integrated temperature profile, including geological storage 72
Scheme of the open cycle paired with geological storage and carbon capture 73
Trend of temperatures as function of heat flow for the evaporator of the charge cycle 78
Trend of temperatures as function of heat flow for the condenser of the discharge cycle 78
Trend of temperatures as function of heat flow for the evaporator of the charge cycle 82
Trend of temperatures as function of heat flow for the condenser of the discharge cycle 82
Trend of temperatures as function of heat flow for the evaporator of the charge cycle 83
Trend of temperatures as function of heat flow for the condenser of the discharge cycle 84
Scheme of a basic absorption chiller 85
Scheme of the closed cycle paired with the absorption chiller cycle on the discharge part 86
Trend of temperatures as function of heat flow for the condenser of the discharge cycle 89
Scheme of cascade transcritical, single-stage (top) and transcritical, single-stage (bottom)..... 90
Expected trends for the configuration reported in Figure 24 90
Scheme of the close cycle paired with cascade heat pump on the charge part..... 91

Acronyms and Abbreviations

- **TES -** Thermal Energy Storage
- **CFCs -** Chlorofluorocarbons
- **HFCs** - Hydrofluorocarbons
- **HP -** Heat Pump
- **HE -** Heat Engine
- **LT -** Low Temperature
- **HT -** High Temperature
- **CV -** Control Volume
- **H_2O -** Water
- **CO_2, R-744 -** Carbon Dioxide
- **C_3H_8, R-290 -** Propane
- **NH_3, R-717 -** Ammonia
- **M -** Molar Mass
- **NBP -** Normal Boiling Point
- **TEWI -** Total Equivalent Warming Impact

1. Introduction

Since the beginning of civilization renewable energy sources have played a crucial role in human history allowing social and technological development. Nowadays the choice of investing on renewable energy to meet the present energy demand is justified by environmental reasons, particularly with the aim of reducing local and global atmospheric emissions [1]. Although often commercially available, most are still at an early stage of development and not technically mature and only few renewable energy technologies can actually compete with conventional fuels on cost. But substantial cost reductions can be achieved for most renewables, closing gaps and making them more competitive.

The development of renewable energy is strongly connected to the implement of efficient ways to store energy to correct the mismatch between supply and demand of energy. The focus in this thesis is on sensible TES that allows to store thermal energy to be used subsequently for producing electricity. In order to do that a reversible HP that works with CO_2 is used. The choice of this working fluid is justified by its unique thermo-physical properties and the need for limiting its emissions from the use of fossil fuels. To achieve this goal, other feasible options are represented by the capture and the storage of CO_2 in geological formation.

The main idea so, is to develop a cross-sectoral technology for the energy transition, combining a renewable energy storage system based on the transcritical CO_2 cycle, CO_2 storage in geological formations and geothermal heat extraction. In Europe the CEEGS (CO_2 based electrothermal energy and geological storage system) project has the objective to provide scientific proof of the techno-economic feasibility of this technology, raising the current low Technology Readiness Level (TRL) from 2 to 4 by addressing gaps in the interface between surface trans-critical cycle and the subsurface CO_2 storage.

Different studies have been carried out to meet the objective of the CEEGS project, in particular the work executed by A. Carro, R. Chacartegui, C. Ortiz, J. Carneiro and J.A. Becerra presents an energy storage system based on transcritical CO_2 cycle. The system proposed is based on the concept of electrothermal energy storage and its integration with geological CO_2 storage. The paper develops the concept and analyses the different modes of operation

by carrying out a dimensioning of the plant. Mosty of the input parameters used for the modelling part of this thesis are taken from this study [2].

The aim of this thesis is to model and analyse a close cycle based on a reversible HP that works with transcritical CO_2. This system stores thermal energy in the charge cycle that can be used in the discharge one to produce electrical energy. An exergo-economic analysis of the system is performed to highlight the total system costs in monetary terms and any thermodynamic analysis of the system, including the initial investment and maintenance costs of the assessment [3]. It is crucial to the design and operation of a cost-effective system. In fact, it provides extra information than exergy analysis for the design of cost-effective energy systems, as an exergy-aided cost-reduction method, by associating costs with exergy losses. It aims to calculate separately the costs of each product generated by a system having more than one product, to understand the cost-formation process and the flow of costs in the system, to optimize specific variables in a single component, or to optimize the overall system.

In addition, different integration scenarios are proposed to improve the power production or to solve some technical limitation of the base case. The first integration suggested is an open cycle based on a reversible HP that works with transcritical CO_2, paired with geological storage. Then two different LT scenarios are presented. In the first one various refrigerants are compared using the base case configuration to find the most suitable one. In the second one the base case configuration is paired with and absorption chiller cycle that works with NH_3-H_2O solution. Lasty, for the HT scenario a configuration based on a cascade HP with a transcritical bottom cycle and a transcritical top cycle for the charge part is presented.

2. Electrothermal energy storage using transcritical CO2 cycles

Energy storage is used to decouple the power supply from the power demand maintaining grid frequency and power quality and allowing a flexibility in the choice of fuels and primary energy sources [4]. Different storage technologies are used in electric power systems such as chemical, electrochemical, mechanical, electromagnetic, or thermal storage. In this classification, the conversion step before the storage is defined as direct or indirect, depending on if source energy has been converted to other forms of energy before storage [5].

An electrothermal energy storage system, during period of excess of electricity generation, in the so-called charge phase, converts electric energy into thermal energy, storing it in insulated tanks. On the other hand, during the discharge phase, in periods of electricity deficit, the thermal energy is extracted and converted into electric energy. The thermal storage (TES) can be based on sensible, latent (PCM) or thermo-chemical (TCS) heat storage [6].

To store thermal energy, in the system under analysis, a reversible HP is used, and it is composed by two cycles indirectly connected by the heat storage tanks. Each cycle is a supercritical one with CO_2 as working fluid and it can be closed or open. In open case the cycle is coupled with an underground geological storage to store the carbon dioxide in such a way that it cannot escape into the atmosphere [7].

2.1 Transcritical or supercritical cycle

The transcritical or supercritical cycle is a cycle with a maximum pressure higher than the critical one [8].

According to the study effectuated by Feher [9], it is characterized by high thermal efficiency, low volume to power ratio, no blade erosion in the turbine, no cavitation in the pump, single stage turbine and pump, single phase fluid in the heat rejection process, and insensitivity to compression efficiency.

The use of supercritical CO_2 as a working fluid is a choice that was popular in the first twenty years of the 20th century especially for refrigerant purposes. But due to poor technology at the time, the physical properties of this fluid (the very low critical temperature, 31.1 °C and the high critical pressure, 7.37 MPa) and the typology of cooling medium, usually low temperature groundwater or seawater, it results in low refrigeration efficiency and a subcritical cycle for CO_2 system. It was replaced then by synthetic refrigerants [10].

In the last years the interest through this fluid has grown. In fact, the 2015 Paris Agreement and the 2018 Intergovernmental Panel on Climate Change (IPCC) have focused their attention on the atmospheric concentration of greenhouse gases and their effects on the global warming increase. The disastrous consequences on the environmental habitats, due to an increase in temperature above 2 °C, have been investigated and compared to a 1.5 °C increase [11]. Many solutions are presented in Hawken's book to reverse global warming and an important role is played by refrigerants. The most diffuse are chlorofluorocarbons gases (CFCs), that have a deleterious effect on the ozone layer, and hydrofluorocarbons (HFCs), that have a capacity to warm the atmosphere that is thousands to nine thousand greater than that of CO_2. The Montreal Protocol on Substances That Deplete the Ozone layer bans CFCs and the 2016 Kigali Amendment to the Montreal Protocol, adopted from more than 170 countries, phases out HFCs by 2028. Substitutes to these refrigerants are already present on the market, as natural refrigerants such as propane, carbon dioxide or ammonia [12].

The use of CO_2 as a working fluid for supercritical cycle is also justified by its unique thermo-physical properties because it has both the characteristics of gas and liquid. The low critical temperature makes this material adapt to work in cycles with water and the high density leads to a compact equipment and a large power density. It is also characterized by a low surface tension which is responsible for a reduction of the cavitation effect in the machinery and the low compression ratios required, near to the critical point, leads to higher efficiency of the machinery [13]. Moreover, due to the high value of compressibility, a small change in pressure causes large changes in density that affects diffusivity, viscosity, and other properties so the chemical reaction rates can be easily controlled [14]. Also, the environmental properties are excellent because it is non-flammable and non-toxic [15].

The closed-loop supercritical CO_2 cycles can have application in fossil, nuclear and concentrating solar power plants, as well in waste heat recovery and marine systems [16].

2.2 Reversible heat pump

A HP is a machine that transfers heat from a LT source to a HT one, using a refrigeration cycle. In this cycle a refrigerant is firstly compressed with a compressor, then it is condensed releasing heat to the outside and expanded though an expansion valve before entering an evaporator where the heat is absorbed by the outside.

Usually, the HP is used for heating or conditioning an ambient by transferring heat to a space to be heated during winter season and by extracting heat from the same space to be cooled during the summer period [17].

In the system under analysis based on transcritical CO_2, the HP is used to convert the electrical energy in thermal one during the excess of electricity generation and as HE to convert the thermal energy into electrical one during deficit of electricity generation. So, it is composed by two closed cycles, respectively the charge cycle and the discharge one, indirectly connected through the insulated reservoirs. In Figure 1 it is shown the working scheme of the HP (1-2-3-4) and the HE (5-6-7-8). To ensure a high efficiency of the system and to minimize the exergy losses in the heat exchange process is necessary to have close, and if it is possible parallel, curves between the heat exchange process and the storage tanks.

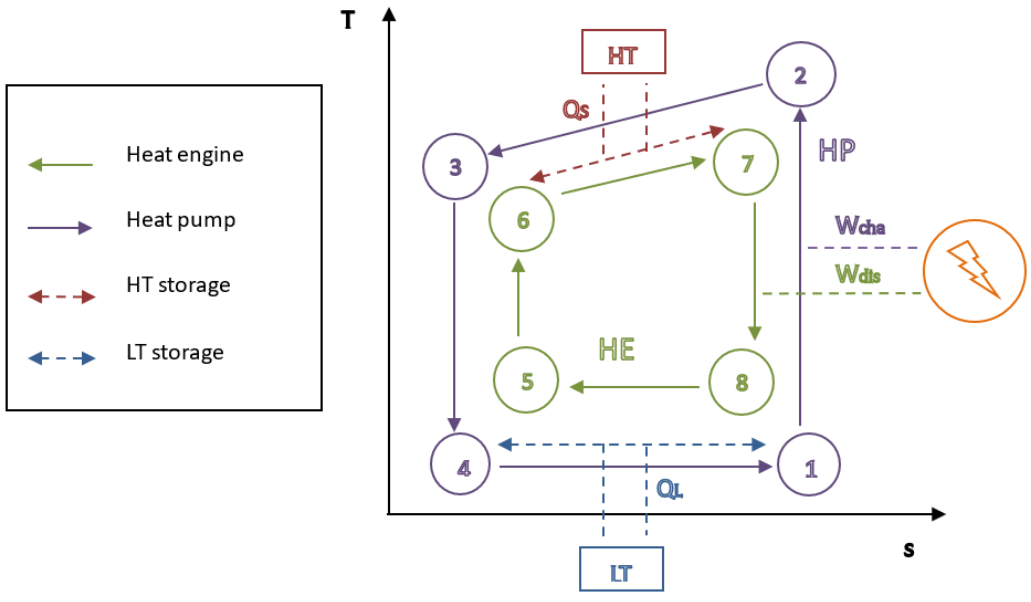

Figure 1. Reversible heat pump energy storage system with well-integrated temperature profile

The operation conditions and working fluid properties allows that the thermal energy is stored as sensible heat in water in the HT side. The theoretical cycle reported in Figure 1 uses latent heat in the LT side to evaporate or to condense the CO_2 but, in the reference system, sensible heat is used due to impossibility of the modelling software, Aspen Hysys®, to work with solid material in the heat exchangers. In fact, H_2O has a very high heat capacity and consequently a high energy density of the storage in both volume and mass. Moreover, it has excellent heat transfer and transport properties and optimal chemical properties such as toxicity, flammability, corrosiveness.

3. Physical structure of the system

In Figure 2 is reported the scheme of the reference system composed of a closed cycle in charge and discharge operation, taken from [2], with all the components and the streams. The charge cycle is located at the left of the scheme while the discharge cycle on the right.

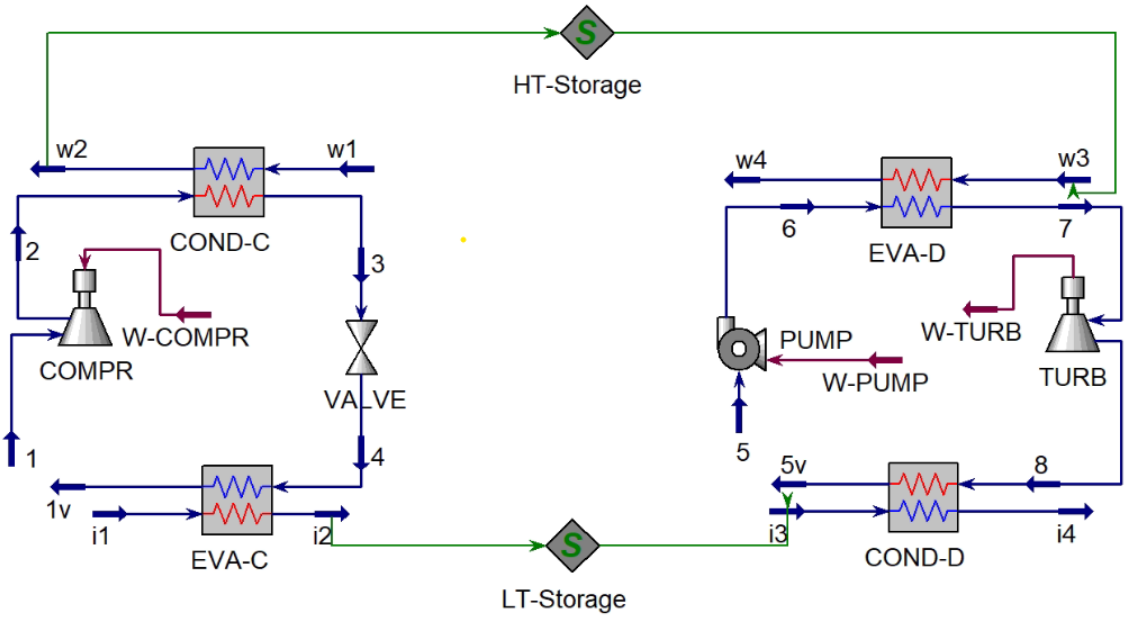

Figure 2. Scheme of the reference system

The charge cycle is composed of the following components:

- *COMPR - Compressor:* it compresses the CO_2 coming from the evaporator increasing the pressure and the temperature values to reach the high-pressure level of the cycle.
- *COND-C - Condenser*: it condenses the hot CO_2 exchanging heat with the H_2O. The H_2O enters the cold side of the heat exchanger receiving the heat released from the CO_2. At the end it is stored in a HT tank to be used in the discharge cycle.
- *VALVE - Valve*: it expands the CO_2 to reach the low-pressure level of the cycle. At the exit the fluid is constituted by a vapour and a liquid phase.
- *EVA-C - Evaporator*: it evaporates the CO_2 until reaching the saturation condition. In this way it is possible avoid damage to the compressor due to liquid droplets [18]. The H_2O enters the hot side of heat exchanger and releases sensible heat to the CO_2. Then it is stored in a LT tank to be used in the discharge cycle.

The discharge cycle is composed of the following components:

- *PUMP - Pump*: it increases the pressure and the temperature of the CO_2, coming from the condenser, to reach the high-pressure level of the cycle.
- *EVA-D - Evaporator*: it evaporates the CO_2 absorbing the heat released by the H_2O. The H_2O comes from the HT tank, and it enters the hot side of the heat exchanger. At the end it is released in the environment.
- *TURB - Turbine*: it expands the CO_2 to reach the low-pressure level of the cycle.
- *COND-D - Condenser*: it condenses the CO_2 to the saturation condition releasing heat to the H_2O. In fact, the water coming from the LT storage, enters the cold side of the heat exchanger and it is heated up.

In order to proceed with the analysis of the plant a CV has to be defined to underline the part of the system of interest. In fact, the exergo-economic analysis is performed on the part of the system comprised inside the CV. The CV can be chosen arbitrarily. For the system under investigation the choice is justified by the successive change of the refrigerant fluid used for storage and by a willingness to simplify reducing the number of analysed streams. In Figure 3 is reported a scheme of the closed cycle in which the CV is highlighted.

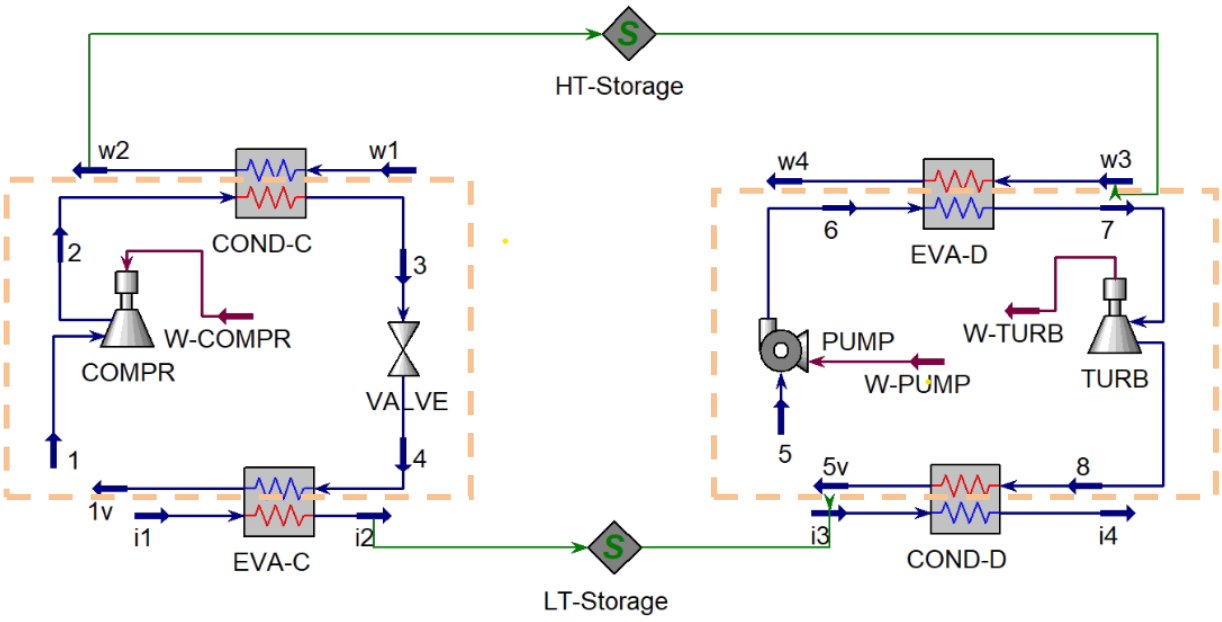

Figure 3. Scheme of the reference system highlighting the control volume

After the definition of the CV it is possible to identify the streams that interact with it and the components comprised inside it. In order to describe the structure of the system (the one comprised inside the CV) the incidence matrix A is defined. It is a $(n \times m)$ matrix where n is the number of components and m is the number of the total streams, both energy and mass ones. For the system considered the number of components n is equal to 8 while the number of streams m is equal to 15. The number of streams, beyond considering the mass ones, considers also the power needed by the compressor and the pump, the power released by the turbine and the heat flux absorbed or released by each heat exchanger.

This incidence matrix, reported in Table 1, is built on the following rules:

- If the considered stream enters the component, then the value for that component is equal to 1.
- If the considered stream exits the component, then the value for that component is equal to -1.
- If the considered stream doesn't enter or exit the component, then the value for that component is equal to 0.

Table 1. Incidence matrix of the considered system

	Mass Streams								*Energy Streams*						
	1	*2*	*3*	*4*	*5*	*6*	*7*	*8*	*W-COMPR*	*W-PUMP*	*W-TURB*	*Φ-COND-C*	*Φ-EVA-C*	*Φ-EVA-D*	*Φ-COND-D*
COMPR	1	-1	0	0	0	0	0	0	1	0	0	0	0	0	0
COND-C	0	1	-1	0	0	0	0	0	0	0	0	-1	0	0	0
VALVE	0	0	1	-1	0	0	0	0	0	0	0	0	0	0	0
EVA-C	-1	0	0	1	0	0	0	0	0	0	0	0	1	0	0
PUMP	0	0	0	0	1	-1	0	0	0	1	0	0	0	0	0
EVA-D	0	0	0	0	0	1	-1	0	0	0	0	0	0	1	0
TURB	0	0	0	0	0	0	1	-1	0	0	-1	0	0	0	0
COND-D	0	0	0	0	-1	0	0	1	0	0	0	0	0	0	-1

In steady state conditions the balance of mass (Formula 1), energy (Formula 2) and exergy (Formula 3) are expressed in matrix form as follows.

$$A \times M = 0 \quad (1)$$

$$A \times U = 0 \quad (2)$$

$$A \times E = I \quad (3)$$

Where:

- A is the $(n \times m)$ incidence matrix.
- M, U, E are $(m \times 1)$ vectors containing respectively the values of mass flow rate, energy and exergy for each stream.
- I is the $(n \times 1)$ irreversibility vector defined for each component.

4. Productive structure of the system

In order to perform a complete definition of the system under analysis the productive structure is investigated. The productive model of the plant considers the productive purposes of the process units with the definition of the fuels and products and the distribution of the resources throughout the plant. The definition of these quantities is not unique and it depends, for each component, from its operational role in the process and from the identified CV. Resources and products can be defined as the sum or difference of physical flows, both mass and energy ones.

The system under investigation has the purpose, on the charge side, to store the sensible heat in a HT and LT tank and, on the discharge side, to convert the stored heat in electrical energy. With this assumption the Table 2 is built reporting the productive purpose of each component.

Table 2. Productive structure of the whole system

Component	*Resource*	*Product*	*Loss*
COMPR	W_{COMPR}	$E_2 - E_1$	/
COND-C	$E_2 - E_3$	Φ_{COND-C}	/
VALVE	E_3	E_4	/
EVA-C	$E_4 - E_1$	$\Phi_{\mathrm{EVA-C}}$	/
PUMP	W_{PUMP}	$\mathrm{E}_6 - \mathrm{E}_5$	/
EVA-D	Φ_{EVA-D}	$\mathrm{E}_7 - \mathrm{E}_6$	/
TURB	$E_7 - E_8$	$\mathrm{W}_{\mathrm{TURB}}$	/
COND-D	Φ_{COND-D}	$\mathrm{E}_5 - E_8$	/

5. Aspen Hysys® modelling

The steady state simulation is executed with Aspen Hysys® a software that uses sequential-modular approach for solving the flowsheet, in which each unit operation is considered as a separate block and calculated sequentially [19].

Starting with some input data, reported in Tables 4 and 5, and specifying an appropriate property method, Aspen Hysys® predicts the outputs for a designed process, defining the thermodynamic state for each node of the model.

The property methods selected for each fluid are shown in the Table 3.

Table 3. Property methods used for each fluid

Fluid	*Property Method*
CO_2	PENG-ROB
H_2O	PENG-ROB

The most important characteristics of the chosen method are reported [20]:

- *PENG-ROB*: it uses the Standard Peng-Robinson cubic equation of state for all the thermodynamic properties except liquid molar volume and the API method for liquid molar volume of pseudocomponents and the Rackett model for real components. This method is indicated for nonpolar or mildly polar mixtures such as hydrocarbons and light gases, such as carbon dioxide, hydrogen sulphide and hydrogen. It can be used at all temperatures and pressures and it is consistent in the critical region even if the results are least accurate in the region near the mixture critical point.

For the selection of the input data, a pressure range of 140 to 200 bar is chosen as the most suitable for high CO_2 pressure values in the transcritical cycle. This selection is based on the principle that higher pressure during the charging phase results in a higher compressor outlet temperature, which significantly influences the turbine inlet temperature during the discharge cycle. This temperature, along with the discharge pressure, determines the available enthalpy change. At lower pressures, a CO_2 saturation temperature of 0 °C corresponds to a pressure of about 35 bar. Regarding system performance relative to low-pressure values, the highest feasible low-pressure value during charging minimizes the work of the compressor, while the

lowest feasible pressure during discharge maximizes the output of the turbine. Therefore, the low-pressure operating range should balance these conditions and ensure efficient heat exchange with the LT tank. By establishing a minimum temperature difference of 4 °C in the heat exchanger and neglecting the pressure drop, the selected low-pressure range is 30–40 bar. This range sets the maximum vaporization pressure of CO_2 during charging at 30 bar and the minimum condensation pressure of CO_2 during discharge at 40 bar, optimizing system performance.

The system is constructed adding all the components explained before and inserting the input parameters that are summarized in Tables 4 and 5. A "break point" is considered in the model for the cycle input conditions and it is inserted at state points 1 and 5.

Table 4. Main assumptions, inputs and hypothesis on the modelling of the charge cycle for the base case

Input parameters charge cycle

COMPR	Isentropic Efficiency	0,86	-
	Inlet Vapor fraction	1	-
	Inlet Pressure	30	bar
	Power	1	MW
	Outlet Pressure	200	bar
COND-C	Min Approach Temperature	4	°C
	Pressure Drop	0	bar
	Inlet Temperature Cold Side	30	°C
	Inlet Pressure Cold Side	12	bar
VALVE	Inlet Temperature	70	°C
EVA-C	Min Approach Temperature	4	°C
	Pressure Drop	0	bar
	Inlet Temperature Hot Side	10	°C
	Inlet Pressure Hot Side	5	bar

Table 5. Main assumptions, inputs and hypothesis on the modelling of the discharge cycle for the base case

Input parameters discharge cycle

PUMP	Isentropic Efficiency	0,85	-
	Inlet Liquid fraction	1	-
	Inlet Pressure	40	bar
	Power	1	MW
	Outlet Pressure	190	bar
EVA-D	Min Approach Temperature	4	°C
	Pressure Drop	0	bar
	Inlet Temperature Hot Side	161	°C
	Outlet Temperature Hot Side	30	°C
	Inlet Pressure Hot Side	12	bar
TURB	Isentropic Efficiency	0,88	-
	Outlet Pressure	40	bar
COND-D	Min Approach Temperature	4	°C
	Pressure Drop	0	bar
	Inlet Temperature Cold Side	-1,046	°C
	Inlet Pressure Cold Side	5	bar

6. Energy analysis

An energy analysis is performed for each component of the charge cycle to verify the coherence of the outputs and the specific thermodynamic equations are reported for the reference conditions.

- *Compressor*: the energy balance has as an input values the isentropic efficiency and the power. Considering that it is known also the vapor fraction and the pressure at the inlet, it is possible to determine the position of the inlet point on the saturation curve of the CO_2 obtaining all the thermodynamic properties of this point. The equations used are reported:

$$G_1 \cdot h_1 + W_c - G_2 \cdot h_2 = 0 \quad (4)$$

$$\beta_c = \frac{p_2}{p_1} \quad (5)$$

$$\eta_{c,is} = \frac{h_{2,is} - h_1}{h_2 - h_1} \quad (6)$$

- *Condenser:* the hot side is the one with the CO_2 while the cold one has the H_2O as operating fluid. The energetic balance has as input values the mass flow rate at the hot side, the inlet thermodynamic properties at both sides and the outlet temperature at the hot side. Moreover, the minimum temperature difference at the pinch point is known and the pressure losses, that are negligible. The equations used are reported:

$$G_2 \cdot h_2 - G_3 \cdot h_3 + G_{w1} \cdot h_{w1} - G_{w2} \cdot h_{w2} = 0 \quad (7)$$

$$T_{hot,pinch} = T_{cold,pinch} + \Delta T_{min} \quad (8)$$

- *Valve:* the energy balance has as input values the outlet pressure and the thermodynamic properties at the inlet. The lamination process can be approximated to an iso-enthalpic expansion:

$$h_3 \cong h_4 \quad (9)$$

- *Evaporator:* the hot side is the one with H_2O while the cold one has the CO_2 as operating fluid. The energy balance has as an input values the mass flow rate at the cold side, the inlet thermodynamic properties at both sides and the outlet thermodynamic properties at cold side. Moreover, the minimum temperature difference at the pinch point is known and the pressure losses, that are negligible. The equations used are reported:

$$G_4 \cdot h_4 - G_1 \cdot h_1 + G_{i1} \cdot h_{i1} - G_{i2} \cdot h_{i2} = 0 \quad (10)$$

$$T_{hot,pinch} = T_{cold,pinch} + \Delta T_{min} \quad (11)$$

An energy analysis is also performed for each component of the discharge cycle to verify the coherence of the outputs and the specific thermodynamic equations are reported.

- *Pump:* the energy balance has as an input values the isentropic efficiency and the power. Considering that it is known also the vapor fraction and the pressure at the inlet, it is possible to determine the position of the inlet point on the saturation curve of the CO_2 obtaining all the thermodynamic properties of this point. The equations used, considering negligible the difference in height and velocity between the inlet and the outlet, are reported:

$$\Delta H = \frac{p_6 - p_5}{\rho \cdot g} \quad (12)$$

$$W = \eta_{is} \cdot G \cdot g \cdot \Delta H \quad (13)$$

- *Evaporator:* the cold side is the one with the CO_2 while the hot one has the H_2O as operating fluid. The energy balance has as an input values the mass flow rate at the cold side, the inlet thermodynamic properties at both sides and the outlet thermodynamic properties at hot side. Moreover, the minimum temperature

difference at the pinch point is known and the pressure losses, that are negligible. The equations used are reported:

$$G_6 \cdot h_6 - G_7 \cdot h_7 + G_{w3} \cdot h_{w3} - G_{w4} \cdot h_{w4} = 0 \quad (14)$$

$$T_{hot,pinch} = T_{cold,pinch} + \Delta T_{min} \quad (15)$$

- *Turbine:* the energy balance has as an input values the thermodynamic properties at the inlet, the pressure at the outlet and the isentropic efficiency. The equations used are reported:

$$G_7 \cdot h_7 - W_t - G_8 \cdot h_8 = 0 \quad (16)$$

$$\beta_{ht} = \frac{p_8}{p_7} \quad (17)$$

$$\eta_{ht,is} = \frac{h_8 - h_7}{h_{8,is} - h_7} \quad (18)$$

- *Condenser:* the cold side is the one with the H_2O while the hot one has the CO_2 as operating fluid. The energy balance has as an input values the mass flow rate at the hot side, the inlet thermodynamic properties at both sides and the outlet thermodynamic properties at hot side. Moreover, the minimum temperature difference at the pinch point is known and the pressure losses, that are negligible. The equations used are reported:

$$G_8 \cdot h_8 - G_5 \cdot h_5 + G_{i3} \cdot h_{i3} - G_{i4} \cdot h_{i4} = 0 \quad (19)$$

$$T_{hot,pinch} = T_{cold,pinch} + \Delta T_{min} \quad (20)$$

The thermodynamic state at each point is obtained and the main output parameters are reported in Table 6. These values are considered while performing the exergo-economic analysis.

Table 6. Thermodynamic state of the mass streams for the reference system

Stream	*m [kg/s]*	*T [°C]*	*p [bar]*	*Vapour fraction [-]*	*h [J/kg]*	*s [J/kgK]*
1	9,525	-5,048	30	1	-9,02E+06	3,07E+03
2	9,525	165	200	1	-8,91E+06	3,11E+03
3	9,525	70	200	0	-9,10E+06	2,61E+03
4	9,525	-5,046	30	0,66	-9,10E+06	2,76E+03
w1	3,136	30	12	0	-1,59E+07	3,05E+03
w2	3,136	161	12	0	-1,53E+07	4,63E+03
i1	17,02	10	5	0	-1,60E+07	2,76E+03
i2	17,02	-1,047	5	0	-1,60E+07	2,59E+03
5	50,75	5,594	40	0	-9,24E+06	2,24E+03
6	50,75	22,66	190	0	-9,22E+06	2,25E+03
7	50,75	157	190	1	-8,92E+06	3,10E+03
8	50,75	28,67	40	1	-8,99E+06	3,13E+03
w3	26,27	161	12	0	-1,53E+07	4,63E+03
w4	26,27	30	12	0	-1,59E+07	3,05E+03
i3	959,8	-1,047	5	0	-1,60E+07	2,59E+03
i4	959,8	2	5	0	-1,60E+07	2,63E+03

7. Exergo-economic analysis

The Exergy Balance equation is written for each component j connected to the stream k:

$$\sum_j \left(1 - \frac{T_0}{T_j}\right) \Phi_j - W_{t,j} = \left(\frac{dA_j}{dt}\right)_{CV} + \sum_k G_k \cdot (b + \zeta)_k + \Psi_j \qquad (21)$$

Where:

- T_0 is the ambient temperature and T_j is the temperature of the j component.
- Φ_j is the thermal power exchanged.
- $W_{t,j}$ is the technical power of the j component.
- $\left(\frac{dA_j}{dt}\right)_{CV}$ is the variation with time of the internal exergy of the control volume.
- G_k is the mass flow rate of the k stream.
- b_k is the specific physical exergy of the k stream.
- ζ_k is the specific chemical exergy of the k stream.
- Ψ_j is the exergy destroyed within component j.

The external reference environment is chosen between the temperatures at the evaporator and the condenser of the charge and discharge cycle, with the following conditions:

$$T_0 = 25°C \text{ e } p_0 = 1\ bar$$

To use the Formula 21, it is necessary to estimate the specific physical and chemical exergy for each mass stream, mixture of different i components, using Formulas 22 and 23 [21].

$$b = (h - h_0) - T_0 \cdot (s - s_0) \qquad (22)$$

$$\zeta = \sum_i x_i b_i^{ch,0} + RT_0 \sum_i x_i \ln x_i \qquad (23)$$

Where:

- h and s are respectively the enthalpy and the entropy of the considered stream.
- h_0, s_0 and T_0 are respectively the enthalpy, the entropy and the temperature of the external reference environment.
- x_i is the molar fraction of the single component i present in the considered stream.
- $b_i^{ch,0}$ is the chemical exergy estimated at the condition of the reference environment of the single component i present in the considered stream [22].
- R is the universal gas constant.

The exergy E is a $(m \times 1)$ vector containing all the exergy flows of the system. It has a number of rows equal to the m number of streams, energy and mass ones. It is reported in Table 7.

Table 7. Exergy vector

	E [MW]
1	6,05
2	6,96
3	6,55
4	6,15
5	33,61
6	34,48
7	36,83
8	32,80
W-COMPR	1,00
W-PUMP	1,02
W-TURB	3,55
Φ-COND-C	0,35
Φ-EVA-C	-0,06
Φ-EVA-D	2,90
Φ-COND-D	-1,13

The irreversibility I is a $(n \times 1)$ vector containing the exergy destroyed in each component. It has a number of rows equal to the n number of components and it can be estimated according to Formula 3, reported below.

$$I = A \times E$$

Where:

- A is the $(n \times m)$ incidence matrix, reported in Table 1.
- E is the $(m \times 1)$ exergy vector, reported in Table 7.

The total irreversibility of the charge cycle is equal to 0,59 MW while the one of the discharge cycle is equal to 1,50 MW. The difference between these two values is justified mainly by the difference between the mass flow rates of the two cycles. The obtained irreversibility vector is reported in Table 8.

Table 8. Irreversibility vector

	I [MW]
COMPR	0,10
COND-C	0,06
VALVE	0,41
EVA-C	0,03
PUMP	0,15
EVA-D	0,54
TURB	0,48
COND-D	0,32

The percentages of exergy destroyed calculated for each component and referred to the total irreversibility for each cycle, at the reference conditions, are shown in Figure 4.

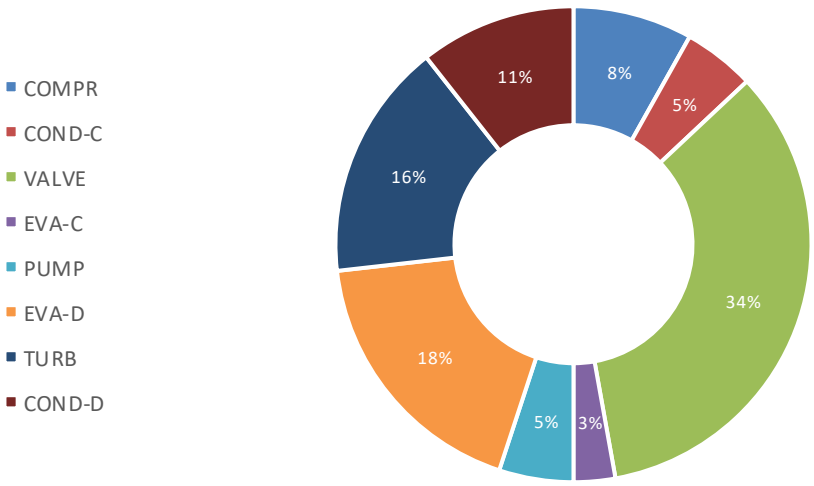

Figure 4. Exergy destroyed percentages associated at each component

7.1 Exergy cost analysis

In every energy system, the exergy of the resources is greater than or equal to that of the products. For both the plant as a whole as well for the single component the amount of exergy needed to obtain the products (P) is equal to the exergy of the resources (F) consumed plus the irreversibilities (I).

$$F - P = I > 0$$

The exergy cost E^* associated with a physical flow is the amount of exergy needed to produce this flow, equal to sum of exergy and all the accumulated irreversibilities produced. The exergy cost is related to the production process, linked to a set of internal and external conditions. Moreover, it is important to define the unit exergy cost k^*, obtained by the ratio between the exergy cost and the exergy defined for a certain i stream. It is defined as the amount of exergy associated to the external resource to produce a unit exergy associated with a specific flow.

$$k_i^* = \frac{E_i^*}{E_i} \qquad (24)$$

The exergy cost is a conservative property defined by the following balance equation:

$$A \times E^* = 0 \qquad (25)$$

Where:

- A is the $(n \times m)$ incidence matrix, reported in Table 1.
- E^* is the $(m \times 1)$ exergy cost vector with the number of rows equal to the number of streams.

In order to compute the exergy cost of the different streams auxiliary equations are written. Their number is given by the difference $m - n$ where m is the number of the streams and n is

the number of the components. For the system considered the number of streams m is equal to 15 while the number of components n is equal to 8. The $m - n$ difference is equal to 7.

To define them the cost allocation rules $(P1, P2, P3, P4)$ are used:

- *P1*: the first rule regards the flows entering the system. In absence of specific external assessment, the exergy cost of inlet flows is equal to their exergy. The unit cost of resources then is equal to one.

$$k_i^* = \frac{E_i^*}{E_i} = 1$$

$$E_i^* = E_i$$

- *P2:* the second rule regards the discharged flows. In absence of specific external assessment, the exergy cost of waste flows is equal to zero.

$$E_i^* = 0$$

- *P3:* the third rule regards the outlet flows of a specific component that are also partially a resource of that component. The unit exergy cost of the outlet flow is the same of the inlet one. Alternatively, it can be used when the resource of a component is defined as difference of two streams $(E_1 - E_2)$, in this case the unit exergy cost of the two flows is the same.

$$k_1^* = k_2^*$$

$$\frac{E_1^*}{E_1} = \frac{E_2^*}{E_2}$$

$$\frac{E_2}{E_1} \cdot E_1^* - E_2^* = 0$$

- *P4*: the fourth rule regards components that have products composed of several flows with the same thermodynamic quality. The unit exergy cost of these flows is the same. Alternatively, when the product of a component is defined as sum of two streams $(E_1 + E_2)$, the unit exergy cost of the two ones is the same.

$$k_1^* = k_2^*$$

$$\frac{E_1^*}{E_1} = \frac{E_2^*}{E_2}$$

$$\frac{E_2}{E_1} \cdot E_1^* - E_2^* = 0$$

In the system under analysis these rules are used to determine the 7 additional equations needed considering the productive structure summarized in Table 2.

- *P1 at COMPR*. The resource for this component is defined as the power delivered to it. The exergy cost of the inlet energy stream is equal to its exergy.

$$E^*_{W-COMPR} = E_{W-COMPR} = 1{,}00$$

1. *P1 at PUMP*. The resource for this component is defined as the power delivered to it. The exergy cost of the inlet energy stream is equal to its exergy.

$$E^*_{W-PUMP} = E_{W-PUMP} = 1{,}02$$

2. *P1 at EVA-D*. The resource for this component is defined as the heat delivered to it. The exergy cost of the inlet energy stream is equal to its exergy.

$$E^*_{\Phi-\mathrm{EVA-D}} = E_{\Phi-\mathrm{EVA-D}} = 2{,}90$$

3. *P1 at COND-D*. The resource for this component is defined as the heat delivered to it. The exergy cost of the inlet energy stream is equal to its exergy and it has a negative value because the heat is rejected.

$$E^*_{\Phi-\mathrm{COND-D}} = E_{\Phi-\mathrm{COND-D}} = -1{,}13$$

4. *P3 at COND-C*. The resource for this component is defined as the difference $(E_2 - E_3)$. The unit exergy cost of the outlet flow is the same of the inlet one.

$$k_2^* = k_3^*$$

$$\frac{E_2^*}{E_2} = \frac{E_3^*}{E_3}$$

$$\frac{E_3}{E_2} \cdot E_2^* - E_3^* = 0$$

$$0{,}94 \cdot E_2^* - E_3^* = 0$$

5. *P3 at EVA-C.* The resource for this component is defined as the difference $(E_4 - E_1)$. The unit exergy cost of the outlet flow is the same of the inlet one.

$$k_4^* = k_1^*$$

$$\frac{E_4^*}{E_4} = \frac{E_1^*}{E_1}$$

$$\frac{E_1}{E_4} \cdot E_4^* - E_1^* = 0$$

$$0{,}98 \cdot E_4^* - E_1^* = 0$$

6. *P3 at TURB*. The resource for this component is defined as the difference $(E_7 - E_8)$. The unit exergy cost of the outlet flow is the same of the inlet one.

$$k_7^* = k_8^*$$

$$\frac{E_7^*}{E_7} = \frac{E_8^*}{E_8}$$

$$\frac{E_8}{E_7} \cdot E_7^* - E_8^* = 0$$

$$0{,}89 \cdot E_7^* - E_8^* = 0$$

All the previous equations can also be written in matrix formulation:

$$A_c \times E^* = Y_e$$

$$\begin{bmatrix} A \\ \alpha_e \\ \alpha_x \end{bmatrix} \times E^* = \begin{bmatrix} 0 \\ \omega \\ 0 \end{bmatrix} \qquad (26)$$

Where:

- A_c is the $(m \times m)$ cost matrix composed of the incidence matrix A, the matrix α_e that contains the equations related to the P1 and P2 rules and the matrix α_x that contains the equations related to the P3 and P4 rules. It is reported in Table 9.
- E^* is the $(m \times 1)$ exergy cost vector, reported in Table 11.
- Y_e is the $(m \times 1)$ vector that contains the known terms of the equations, reported in Table 10.

Table 9. Cost matrix of the system

	Mass Streams								*Energy Streams*						
	1	2	3	4	5	6	7	8	W-COMPR	W-PUMP	W-TURB	Φ-COND-C	Φ-EVA-C	Φ-EVA-D	Φ-COND-D
COMPR	1	-1	0	0	0	0	0	0	1	0	0	0	0	0	0
COND-C	0	1	-1	0	0	0	0	0	0	0	0	-1	0	0	0
VALVE	0	0	1	-1	0	0	0	0	0	0	0	0	0	0	0
EVA-C	-1	0	0	1	0	0	0	0	0	0	0	0	1	0	0
PUMP	0	0	0	0	1	-1	0	0	0	1	0	0	0	0	0
EVA-D	0	0	0	0	0	1	-1	0	0	0	0	0	0	1	0
TURB	0	0	0	0	0	0	1	-1	0	0	-1	0	0	0	0
COND-D	0	0	0	0	-1	0	0	1	0	0	0	0	0	0	-1
P1	0	0	0	0	0	0	0	0	1	0	0	0	0	0	0
P1	0	0	0	0	0	0	0	0	0	1	0	0	0	0	0
P1	0	0	0	0	0	0	0	0	0	0	0	0	0	1	0
P1	0	0	0	0	0	0	0	0	0	0	0	0	0	0	1
P3	0	0,94	-1	0	0	0	0	0	0	0	0	0	0	0	0
P3	-1	0	0	0,98	0	0	0	0	0	0	0	0	0	0	0
P3	0	0	0	0	0	0	0,89	-1	0	0	0	0	0	0	0

Table 10. Vector of external assessments

	Ye [MW]
COMPR	0,00
COND-C	0,00
VALVE	0,00
EVA-C	0,00
PUMP	0,00
EVA-D	0,00
TURB	0,00
COND-D	0,00
P1	1,00
P1	1,02
P1	2,90
P1	-1,13
P3	0,00
P3	0,00
P3	0,00

Using the inverse of the Equation 26 it is possible to obtain the exergy cost vector E^* and the unit exergy cost vector k^* with Equation 24, reported below. The values obtained are reported in Tables 11 and 12.

$$E^* = A_C^{-1} \times Y_e$$

Table 11. Exergy cost vector

	E [MW]*
1	12,82
2	13,82
3	13,02
4	13,02
5	42,16
6	43,17
7	46,08
8	41,03
W-COMPR	1,00
W-PUMP	1,02
W-TURB	5,05
Φ-COND-C	0,80
Φ-EVA-C	-0,20
Φ-EVA-D	2,90
Φ-COND-D	-1,13

Table 12. Unit exergy cost vector

	k [-]*
1	2,1
2	2,0
3	2,0
4	2,1
5	1,3
6	1,3
7	1,3
8	1,3
W-COMPR	1,0
W-PUMP	1,0
W-TURB	1,4
Φ-COND-C	2,3
Φ-EVA-C	3,3
Φ-EVA-D	1,0
Φ-COND-D	1,0

7.2 Cost of components

In order to proceed with the exergo-economic analysis, for each component its cost is evaluated. Firstly, it is necessary to estimate the cost of the base-case and then to correct it considering the type of the equipment, the dimension, the used material and the operating pressure and temperature [23].

The purchased cost of the equipment in the base-case C_p^0, at ambient operating pressure and using carbon steel construction is estimated with Formula 27.

$$C_p^0 = 10^{K_1 + K_2 \log_{10}(A) + K_3 [\log_{10}(A)]^2} \qquad (27)$$

Where:

- A is the capacity or size parameter of the equipment.
- K_1, K_2 and K_3 are three constants taken from the literature that depend on the type of the component [24].

The Bare Erected Cost (BEC) of the equipment C_{bec} is estimated with a cost function, a relationship that estimates the purchasing cost of a component using as input one or more reference operating conditions. For most component is used the Formula 28 while for specific components the Formula 29.

$$C_{bec} = C_p^0 \cdot F_p \cdot F_m \quad (28)$$

$$C_{bec} = C_p^0 \cdot (B_1 + B_2 \cdot F_p \cdot F_m) \quad (29)$$

Where:

- C_p^0 is the purchased cost of the equipment in the base-case.
- F_m is the corrective factor related to the operating temperature and the used material of the equipment.
- B_1 and B_2 are two corrective factors used for specific components.
- F_p is the corrective factor related to the operating pressure estimated with Formula 30.

$$F_p = 10^{C_1 + C_2 \log_{10}(P) + C_3 [\log_{10}(P)]^2} \quad (30)$$

Where:

- P is the operating pressure of the component.
- C_1, C_2 and C_3 are constants that depend on the typology of the equipment and on the operating pressure.

The cost functions are defined by lower and upper limits of the independent variables. Outside these ranges the resulting cost could be unrealistic. A scale factor is then applied when the independent variables are outside the ranges using Formula 31.

$$\frac{C_1}{C_0} = \left(\frac{S_1}{S_0}\right)^n \tag{31}$$

Where:

- C_0 and S_0 are respectively the purchasing cost and the maximum or minimum equipment cost attribute in the base-case.
- C_1 and S_1 are respectively the purchasing cost and equipment cost attribute in the real case.
- n is the cost exponent. For thermal process equipment its value is minor than unity, in fact the percentage increase in equipment cost is smaller than the percentage increase in equipment size. In the absence of other cost information its value is considered equal to 0,6 (six-tenths rule). In this analysis its value, taken by literature, is different for each component and reported in Table 13.

Table 13. Cost exponent for each component [24]

Component	*Cost exponent*
Compressor	0,95
Heat-Exchanger	0,4
Hydraulic Turbine	0,45
Pump	0,84
Turbine	0,65

Moreover, the purchasing equipment cost, obtained with Formula 27, refers to the year 2001 so it is important to convert this cost into one accurate for the present time that takes into account changing economic conditions. Specific cost indices are defined to make this conversion.

$$\frac{C_1}{C_0} = \frac{I_1}{I_0} \tag{32}$$

Where:

- C_1 and C_0 are respectively the purchasing cost in the real case and in the base one.
- I_1 and I_0 are respectively the cost index referred to the actual case and to the base one. Several cost indices can be used to adjust for the effect of time. The most used for this kind of analysis are the Marshall and Swift Equipment Cost Index (MSECI) and the Chemical Plant Cost Index (CEPCI). In this analysis, the second index is used and its value referred to the years 2001 and 2022 is reported.

$$I_{0,2001} = 394$$

$$I_{1,2022} = 815{,}98$$

The CEPCI consists of a composite index assembled from a set of four sub-indexes: Equipment, Construction Labor, Buildings and Engineering & Supervision. Each index and subindex are the weighted sum of several components. Its value is searched for each month of the year 2022 and then the average is calculated to obtain the final value. The values of the CEPCI for each month are reported in Figure 5 [25].

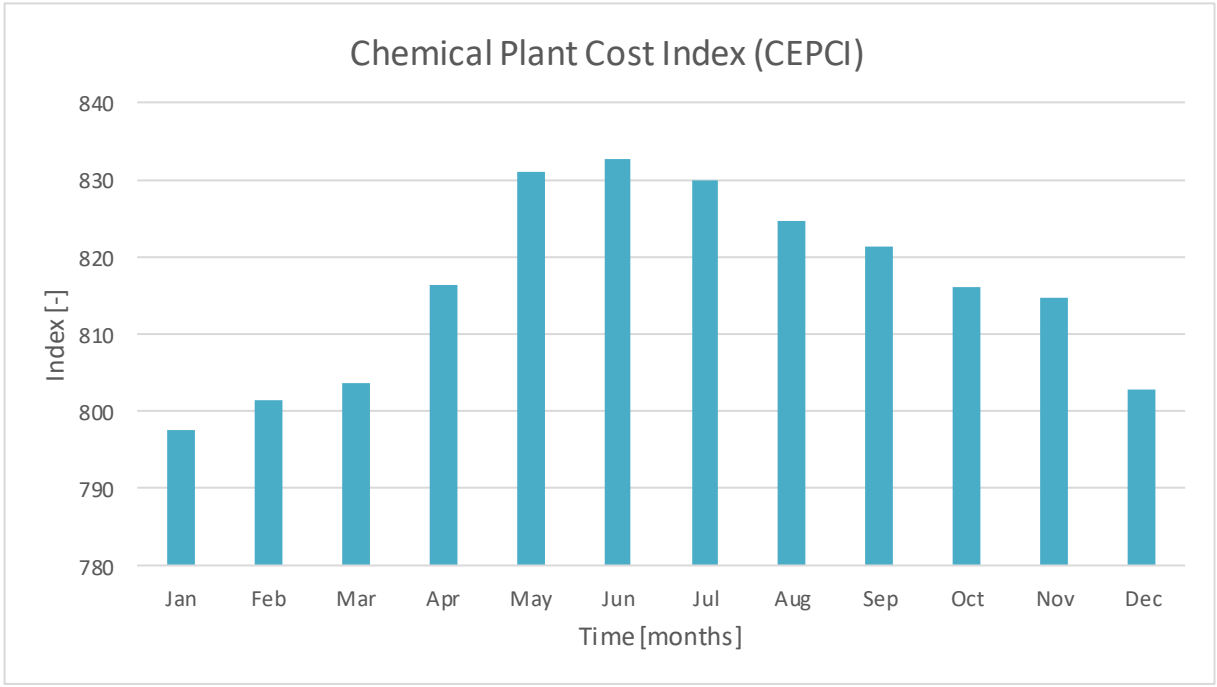

Figure 5. Values of CEPCI for each month of the year 2022

Then the BEC is evaluated for each component of the charge and discharge cycle using the method explained above.

7.2.1 Compressor

Compressors are divided into two categories, positive-displacement and dynamic one [26].

Positive-displacement compressors are characterized by the periodical change of the volume of the working chamber due to mechanical motion of the displacing elements. They can be further classified into two classes based on the motion of the displacer. The first group is the reciprocating compressor, in which the piston executes a sliding action inside the working chamber and the second one is the rotary compressor, whose rotor implements circular or near-circular motion in the working chamber.

Dynamic compressors require the interaction between a continuous flow of working fluid and a set of blades to exchange energy through fluid dynamic action. They can be further classified into two classes according to the direction of fluid flow through the machine. The first group is the centrifugal compressor, that discharges flow in a radial direction and the second one is the axial one, that discharges flow in axial direction, parallel to the compressor axis [27].

The category of compressors more indicated for the considered system is the dynamic one, both the centrifugal and axial classes, due to the high compression ratio required. The software used, Aspen Hysys®, considers for the simulation only the reciprocating and the centrifugal type of compressor. For this reason, the centrifugal compressor is chosen.

Typology	*Parameter*	*Value [kW]*	*K1*	*K2*	*K3*	*Min [kW]*	*Max [kW]*
Centrifugal, axial and reciprocating	Fluid power [kW]	1000	2,2897	1,3604	-1,1027	450	3000

The cost of the compressor is analysed using Turton cost functions. The base cost is estimated using Formula 27.

$$C_p^0 = 10^{K_1 + K_2 \log_{10}(A) + K_3 [\log_{10}(A)]^2} = 279\ 666\ \$$$

Considering that the parameter value, the fluid power, is inside the valid range it is not necessary to apply any correction for the size of the component. Only the correction for time is applied.

$$C_{p,correct}^{0} = \left(\frac{I_1}{I_0}\right) \cdot C_p^0 = \left(\frac{815{,}98}{394}\right) \cdot 279\ 666 = 579\ 196\ \$$$

The corrected factor related to the operating pressure is $F_p = 1$ because for compressors $C_1 = C_2 = C_3 = 0$. The corrected factor related to the operating temperature and the used material of the centrifugal compressor is reported in Table 14.

Table 14. Corrected factor related to temperature and material for centrifugal compressor

Material	*Temperature [°C]*	*Fm*
CS	<430	2,7
SS	<1200	5,7
Ni Alloy	<1000	3,8

Considering that the maximum temperature reached by the working fluid is 165 °C, the used material for the compressor is the Carbon Steel (CS) with a corrected factor $F_m = 2{,}7$.

The BEC obtained, that considers all the corrections, is estimated using Formula 28.

$$C_{bec} = C_{p,correct}^{0} \cdot F_m \cdot F_p = 579\ 196\ \cdot 2{,}7 \cdot 1 = 1\ 563\ 829\ \$$$

7.2.2 Pump

Like compressors, pumps are divided into two main categories according to their principle of operation, positive-displacement or dynamic. In positive displacement pumps, pressure is developed by trapping a quantity of liquid in a chamber and then compressing it to the discharge pressure. In a dynamic pump, the fluid first acquires kinetic energy which is then converted to pressure.

Positive displacement pumps are further classified into two groups, reciprocating and rotary pumps. Rotary pumps, as contrasted to reciprocating pumps, produce a smooth-flowing discharge and do not require check valves at the inlet and discharge sides of the pump to

prevent backflow. Rotary pumps rotate at higher speeds than reciprocating pumps, and thus they can deliver a higher flow rate but at the expense of delivering lower pressures than reciprocating pumps.

Dynamic pumps are classified into two main classes, centrifugal and peripheral pumps and are characterized by their ability to deliver high flow rates at low pressures [28].

Centrifugal pumps contain an impeller, usually having curved blades that are mounted on a shaft. This typology of pumps is employed where it is required to deliver a high flow rate at a medium pressure.

The peripheral pumps employ a combination of mechanical impulse and centrifugal force to produce high heads at low flow rates.

For cost evaluation, it is considered a reciprocating pump, because of mass flows, pressure ratios and characteristics. A centrifugal pump can also be selected for the application.

Typology	*Parameter*	*Value [kW]*	*K1*	*K2*	*K3*	*Min [kW]*	*Max [kW]*
Reciprocating	Fluid power [kW]	1015	3,8696	0,3161	0,122	0,1	200

The base cost is estimated using Formula 27.

$$C_p^0 = 10^{K_1 + K_2 \log_{10}(A) + K_3 [\log_{10}(A)]^2} = 174\ 950\ \$$$

Considering that the parameter value, the fluid power, is not inside the valid range it is necessary to also apply the correction for the size of the component as well as the correction for time. The value for the cost exponent is taken from Table 13.

$$C_{p,correct}^0 = \left(\frac{S_1}{S_0}\right)^n \cdot \left(\frac{I_1}{I_0}\right) \cdot C_p^0 = \left(\frac{1015}{200}\right)^{0,84} \cdot \left(\frac{815,98}{394}\right) \cdot 174\ 950 \quad = 1\ 417\ 964\ \$$$

The corrected factor related to the operating pressure is considered $F_p = 1$ because the operating pressure, equal to 190 bar, is outside the ranges $P < 10$ [bar] and $10 < P < 100$ [bar]. The corrected factor related to the operating temperature and the used material of the reciprocating pump is reported in Table 15.

Table 15. Corrected factor related to temperature and material for reciprocating pump

Material	*Temperature [°C]*	*Fm*
Cast iron	<350	1
CS	<430	1,5
Cu alloy	<600	1,3
SS	<1200	2,3
Ni Alloy	<1000	3,9
Ti	<600	6,4

Considering that the maximum temperature reached by the working fluid is 22,66 °C, the used material for the compressor is the Cast iron with a corrected factor $F_m = 1$.

The corrective factors B_1 and B_2 for reciprocating pumps are reported and the BEC, that considers all the corrections, is estimated using Formula 29.

$$B_1 = 1{,}89 \quad B_2 = 1{,}35$$

$$C_{bec} = C^0_{p,correct} \cdot \left(B_1 + B_2 \cdot F_p \cdot F_m\right) = 1\ 417\ 964\ \cdot (1{,}89 + 1{,}35 \cdot 1 \cdot 1) = 4\ 594\ 202\ \$$$

7.2.3 Turbine

Gas turbines are available in either the radial or axial-flow design, where the radial-flow design is more indicated for low flow rates and high-pressure differences and the axial-flow types for high flow rates and low-pressure differences (1 to 40 bar). The radial-flow expander consists of inflow and outflow types. In the radial-outflow type, the gas flows from the centre to periphery of the impeller. The radial-inflow expander is similar to a centrifugal compressor used in reverse, that is the gas flows radially inward from the periphery of the impeller, exhausting approximately axially. Similarly, the axial expander resembles an axial compressor where the gas flows through an annular passage in a direction that is parallel to the axis of the shaft.

When the source of high-pressure gas is a process stream, the expander is referred to as a turboexpander. Turboexpanders operate at pressures up to 207 bar with isentropic efficiencies of 75 to 88%.

The category of turboexpanders more indicated for the considered system is the radial one due to the high expansion ratio required.

Typology	*Parameter*	*Value [kW]*	*K1*	*K2*	*K3*	*Min [kW]*	*Max [kW]*
Radial gas	Fluid power [kW]	3552	2,2476	1,4965	-0,1618	100	1500

The base cost is estimated using Formula 27.

$$C_p^0 = 10^{K_1 + K_2 \log_{10}(A) + K_3 [\log_{10}(A)]^2} = 332\ 106\ \$$$

Considering that the parameter value, the fluid power, is not inside the valid range it is necessary to also apply the correction for the size of the component as well as the correction for time. The value for the cost exponent is taken from Table 13.

$$C_{p,correct}^0 = \left(\frac{S_1}{S_0}\right)^n \cdot \left(\frac{I_1}{I_0}\right) \cdot C_p^0 = \left(\frac{3552}{1500}\right)^{0,65} \cdot \left(\frac{815,98}{394}\right) \cdot 332\ 106 = 1\ 204\ 617\ \$$$

The corrected factor related to the operating pressure is $F_p = 1$ because for turbines $C_1 = C_2 = C_3 = 0$. The corrected factor related to the operating temperature and the used material of the turbine is reported in Table 16.

Table 16. Corrected factor related to temperature and material for turbine

Material	*Temperature [°C]*	*Fm*
CS	<430	3,5
SS	<1200	6,1
Ni Alloy	<1000	11,8

Considering that the maximum temperature reached by the working fluid is 157 °C, the used material for the compressor is the Carbon Steel (CS) with a corrected factor $F_m = 3{,}5$.

The BEC obtained, that considers all the corrections, is estimated using Formula 28.

$$C_{bec} = C^0_{p,correct} \cdot F_m \cdot F_p = 1\,204\,617 \cdot 1 \cdot 3{,}5 = 4\,216\,160\ \$$$

7.2.4 Heat exchangers

Heat exchangers are frequently characterized by construction features [29]. Four major construction types are tubular, plate-type, extended surface, and regenerative exchangers. Heat exchangers with other constructions are also available, such as scraped surface exchanger, tank heater, cooler cartridge exchanger, and others.

The tubular heat exchangers are usually built of circular tubes, but the design is very flexible because the core geometry can be changed easily. They are designed for high pressure relative to the environment and high-pressure differences between the fluids. They are primarily used for liquid-to-liquid and liquid-to-phase change heat transfer applications. These exchangers can be further classified as shell-and-tube, double-pipe and spiral tube exchangers.

Shell-and-Tube heat exchangers are built of a bundle of round tubes mounted in a cylindrical shell with tube axis parallel to that of the shell. These exchangers are classified and constructed according to TEMA (Tubular Exchanger Manufacturers Association) standards.

Double-Pipe heat exchangers consist in two concentric pipes with the inner pipe plain or finned. Flow distribution is no problem, and cleaning is done very easily by disassembly. This configuration is also suitable where one or both of the fluids is at very high pressure, but it is commonly used for small capacity applications where the total heat transfer area is 50 m^2 or less.

Spiral tube heat exchangers consist of one or more spirally wound coils fitted in a shell. The heat transfer rate associated with a spiral tube is higher than for a straight tube due to the higher heat transfer area that can be achieved with this configuration. Thermal expansion is no problem, but cleaning is almost impossible.

Plate-type heat exchangers are usually built of thin plates that can be either smooth or have some form of corrugation, and they are either flat or wound in an exchanger. Generally, these exchangers cannot accommodate very high pressures, temperatures, or pressure and temperature differences.

Extended surface heat exchangers use fins with high density on one or both fluid sides to increase the surface area and exchanger compactness. Generally increasing the fin density decreases the heat transfer coefficient associated with fins.

Regenerators are storage-type heat exchangers composed by a matrix, the heat transfer surface, that must be moved periodically into and out of the fixed streams of gases or the gas flows must be diverted through valves to and from the fixed matrix.

The software used to model the system, Aspen Hysys®, only works with plate-type or shell-and-tube heat exchangers. Under the same heat exchange task, plate heat exchangers have a higher heat transfer efficiency and so a lower heat exchange area comparing to shell and tube ones. Moreover, they are easier to clean, easier to disassemble and lighter.

In order to apply the cost function for the heat exchangers, the parameter required is the heat transfer area A. The Formula 33, valid for heat exchangers, is applied.

$$\mathrm{A} = \frac{\Phi}{U \cdot \Delta T_{ml}} \qquad (33)$$

Where:

- Φ is the heat transfer rate.
- U is the global heat transfer coefficient.
- ΔT_{ml} is the logarithmic mean temperature difference. It is dependent on the cold and hot side temperatures at the inlet and the outlet of the heat exchanger.

The values obtained as outputs from the software Aspen Hysys® for each heat exchanger are reported in Table 17. The only parameter calculated using Formula 33 is the heat transfer area A.

Table 17. Main results for the heat exchangers

Component	ΔT_{ml} *[K]*	*Duty [MW]*	*U [kW/m²K]*	*Area [m²]*
COND-C	9,8	1,8	5,5	33,5
EVA-C	8,3	0,8	4,1	23,6
EVA-D	11,2	15,2	24	56,9
COND-D	5,6	12,6	45,7	49,2

The values of the constant related to the operating pressure for plate-type heat exchangers, used to estimate the corrected factor, are reported in Table 18.

Table 18. Pressure factor for plate-type heat exchanger

C1	*C2*	*C3*	*Pressure Range [bar]*
0	0	0	P<19

The values of the corrected factor related to the operating temperature and the used material for plate-type heat exchangers are reported in Table 19.

Table 19. Material factor for plate-type heat exchanger

Material	*Temperature [°C]*	*Fm*
CS	<430	1
Cu	<600	1,4
SS	<1200	2,4
Ni alloy	<1000	2,7
Ti	<600	4,6

To estimate the BEC for heat exchangers the Formula 29 is used and the corrective factors B_1 and B_2 for plate-type heat exchangers are reported.

$$B_1 = 0{,}96 \quad B_2 = 1{,}21$$

Condenser charge cycle

Typology	*Parameter*	*Value [m²]*	*K1*	*K2*	*K3*	*Min [m²]*	*Max [m²]*
Plate type	Area [m²]	33,5	4,6656	-0,1557	0,1547	10	1000

The base cost is estimated using Formula 27.

$$C_p^0 = 10^{K_1 + K_2 \log_{10}(A) + K_3 [\log_{10}(A)]^2} = 61\,345 \text{ \$}$$

Considering that the parameter value, the heat transfer area, is inside the valid range it is not necessary to also apply the correction for the size. Only the correction for time is applied.

$$C_{p,correct}^0 = \left(\frac{I_1}{I_0}\right) \cdot C_p^0 = \left(\frac{815{,}98}{394}\right) \cdot 61\,345 = 127\,047 \text{ \$}$$

The corrected factor related to the operating pressure is considered $F_p = 1$ because the operating pressure, equal to 200 bar, is outside the range $P < 19$ [bar], according to Table 18.

Considering that the maximum temperature reached by the hot side working fluid is 165 °C, the used material for the heat exchanger, according to Table 19, is the Carbon Steel (CS) with a corrected factor $F_m = 1$.

The BEC obtained, that considers all the corrections, is estimated using Formula 29.

$$C_{bec} = C_{p,correct}^0 \cdot \left(B_1 + B_2 \cdot F_p \cdot F_m\right) = 127\,047 \cdot (0{,}96 + 1{,}21 \cdot 1 \cdot 1) = 275\,692 \text{ \$}$$

Evaporator charge cycle

Typology	*Parameter*	*Value [m²]*	*K1*	*K2*	*K3*	*Min [m²]*	*Max [m²]*
Plate type	Area [m²]	23,6	4,6656	-0,1557	0,1547	10	1000

The base cost is estimated using Formula 27.

$$C_p^0 = 10^{K_1 + K_2 \log_{10}(A) + K_3 [\log_{10}(A)]^2} = 55\,391 \text{ \$}$$

Considering that the parameter value, the heat transfer area, is inside the valid range it is not necessary to also apply the correction for the size. Only the correction for time is applied.

$$C_{p,correct}^{0} = \left(\frac{I_1}{I_0}\right) \cdot C_p^0 = \left(\frac{815{,}98}{394}\right) \cdot 55\,391 \; = 114\,716 \; \$$$

The corrected factor related to the operating pressure is considered $F_p = 1$ because the operating pressure, equal to 40 bar, is outside the range $P < 19$ [bar], according to Table 18.

Considering that the maximum temperature reached by the hot side working fluid is 10 °C, the used material for the heat exchanger, according to Table 19, is the Carbon Steel (CS) with a corrected factor $F_m = 1$.

The BEC obtained, that considers all the corrections, is estimated using formula 29.

$$C_{bec} = C_{p,correct}^{0} \cdot \left(B_1 + B_2 \cdot F_p \cdot F_m\right) = 114\,716 \; \cdot (0{,}96 + 1{,}21 \cdot 1 \cdot 1) = 248\,935 \; \$$$

Evaporator discharge cycle

Typology	*Parameter*	*Value [m²]*	*K1*	*K2*	*K3*	*Min [m²]*	*Max [m²]*
Plate type	Area [m²]	56,9	4,6656	-0,1557	0,1547	10	1000

The base cost is estimated using Formula 27.

$$C_p^0 = 10^{K_1 + K_2 \log_{10}(A) + K_3 [\log_{10}(A)]^2} = 73\,958 \; \$$$

Considering that the parameter value, the heat transfer area, is inside the valid range it is not necessary to also apply the correction for the size. Only the correction for time is applied.

$$C_{p,correct}^{0} = \left(\frac{I_1}{I_0}\right) \cdot C_p^0 = \left(\frac{815{,}98}{394}\right) \cdot 73\,958 \; = 153\,169 \; \$$$

The corrected factor related to the operating pressure is considered $F_p = 1$ because the operating pressure, equal to 190 bar, is outside the range $P < 19$ [bar], according to Table 18.

Considering that the maximum temperature reached by the hot side working fluid is 161 °C, the used material for the heat exchanger, according to Table 19, is the Carbon Steel (CS) with a corrected factor $F_m = 1$.

The BEC obtained, that considers all the corrections, is estimated using Formula 29.

$$C_{bec} = C^0_{p,correct} \cdot \left(B_1 + B_2 \cdot F_p \cdot F_m\right) = 153\ 169\ \cdot (0{,}96 + 1{,}21 \cdot 1 \cdot 1) = 332\ 378\ \$$$

Condenser discharge cycle

Typology	*Parameter*	*Value [m²]*	*K1*	*K2*	*K3*	*Min [m²]*	*Max [m²]*
Plate type	Area [m²]	49,2	4,6656	-0,1557	0,1547	10	1000

The base cost is estimated using Formula 27.

$$C^0_p = 10^{K_1 + K_2 \log_{10}(A) + K_3 [\log_{10}(A)]^2} = 70\ 006\ \$$$

Considering that the parameter value, the heat transfer area, is inside the valid range it is not necessary to also apply the correction for the size. Only the correction for time is applied.

$$C^0_{p,correct} = \left(\frac{I_1}{I_0}\right) \cdot C^0_p = \left(\frac{815{,}98}{394}\right) \cdot 70\ 006\ = 144\ 985\ \$$$

C The corrected factor related to the operating pressure is considered $F_p = 1$ because the operating pressure, equal to 30 bar, is outside the range $P < 19$ [bar], according to Table 18.

Considering that the maximum temperature reached by the hot side working fluid is 28,7 °C, the used material for the heat exchanger, according to Table 19, is the Carbon Steel (CS) with a corrected factor $F_m = 1$.

The BEC obtained, that considers all the corrections, is estimated using formula 29.

$$C_{bec} = C^0_{p,correct} \cdot \left(B_1 + B_2 \cdot F_p \cdot F_m\right) = 144\ 985 \cdot (0{,}96 + 1{,}21 \cdot 1 \cdot 1) = 314\ 617\ \$$$

7.3 Techno Economic-Analysis

The BEC defined for each component is not the actual cost of the plant. In order to estimate it the costing methodology proposed by the National Energy Technology Laboratory (NETL), U.S. Department of Energy is adopted [30]. This methodology defines five levels of Capital Cost:

- *Bare Erected Cost (BEC)*: it comprises the cost of process equipment, on-site facilities and infrastructure that support the plant and the direct and indirect labour required for its construction and installation.
- *Engineering, Procurement and Construction Cost (EPCC)*: it comprises the BEC plus the cost of services provided by the engineering, procurement and construction contractor that includes a detailed design, contractor permitting and project construction management costs.
- *Total Plant Cost (TPC)*: it comprises the EPCC plus project and process contingencies.
- *Total Overnight Cost (TOC)*: it comprises the TPC plus all the costs that do not take into account interests and escalation during the construction period, denominated overnight costs.
- *Total As-Spent Capital (TASC)*: it is the sum of all capital expenditures as they are incurred during the capital expenditure period, including their escalation and interests.

To estimate the TASC the percentages reported in Table 20 are considered.

Table 20. Percentages applied on the BEC

Cost	*Percentage*
Engineering, Procurement and Construction Cost (EPCC)	8% of BEC
Process contingencies (TPC)	5% of EPCC
Project contingencies (TPC)	15% of EPCC
Total Overnight Cost (TOC)	20,2% of TPC
Total As-Spent Capital (TASC)	11,4% of TOC

In Table 21 the results obtained for all the levels of the Capital Cost are reported.

Table 21. Results from the BEC to the TASC

Component	*BEC [$]*	*EPCC [$]*	*TPC [$]*	*TOC [$]*	*TASC [$]*
COMPR	156 3829	1 688 935	2 026 722	2 436 120	2 713 838
COND-C	275 693	297 748	357 298	429 472	478 432
EVA-C	248 935	268 850	322 619	387 789	431 996
PUMP	4 594 202	4 961 738	5 954 086	7 156 811	7 972 688
EVA-D	332 378	358 968	430 762	517 776	576 802
TURB	4 216 160	4 553 453	5 464 144	6 567 901	7 316 641
COND-D	314 618	339 787	407 745	490 109	545 982

7.4 Financial Analysis

The present value is the value of an expected income stream determined as the date of valuation. The present value is always less or equal to the future one because money has an interest-earning potential, a characteristic referred to as the time value of money. During times of negative interest rates then the present value will be less than the future one.

For a uniform series the present value x is estimated with Formula 34.

$$x = y \cdot \frac{i \cdot (i+1)^n}{(i+1)^n - 1} \tag{34}$$

Where:

- y is the TASC of each component.
- n is the life of the plant.
- i is the real discount rate.

Since the lifetime of the investment is quite long, in fact the life of the plant is assumed to be equal to 30 years, the financial analysis is performed in constant currency. In this condition the real discount rate is considered equal to the Weighted Average Cost of Capital (WACC). The estimation of the WACC is based on the financial structure of the investment, a low risk IPP type (Independent Power Production) investment according to NETL methodology [30].

$$WACC = K_e \cdot \frac{E}{D+E} + K_d \cdot \frac{D}{D+E} \quad (35)$$

Where:

- E is the market value of equity.
- D is the market value of debt.
- K_e is the cost of equity, estimated with Formula 36.
- K_d is the cost of debt, estimated with Formula 37.

The Cost of Equity K_e accounts two components, the specific risk of a certain investment and a systemic risk, that depends on the evolution of the economy as a whole. Its value should be then at least equal to the systemic risk.

$$K_e = R_f + \beta \cdot (R_m - R_f) \quad (36)$$

Where:

- R_f is the systemic risk of the investment (risk free) assumed equal to the government bond at short term since it is less risky investment [31].
- R_m is the market return [31].
- β is the sensitivity of a specific investment rate of return to the market modification.

The Cost of Debt K_d is also estimated.

$$K_d = IRS + spread \quad (37)$$

Where:

- IRS is the Interest Rate Swap and it is a fixed interest rate equivalent to a variable interest rate [32].

- $spread$ is the increase of the interest rate depending on the capability of the investor to return the capital [33].

All the values of the parameters used for the financial analysis to estimate the present value are reported in Table 22. They are referred to the country of Spain for the year 2022.

Table 22. Summary of the parameters used for the financial analysis

Parameter	*Value*
n	30
β	1,00
R_f	1,25
$R_m - R_f$	7,49
IRS	1,23
$spread$	1,74
K_e	8,74
K_d	2,97
E	0,30
D	0,70
$WACC$	5%

Using Formula 34 it is possible to estimate the present value of each component spreading the investment (TASC) over the life of the plant. The values obtained are reported in Table 23.

Table 23. Present value estimated on the 30 years of life of the plant

Component	*Present Value [$]*
COMPR	170 568
COND-C	30 070
EVA-C	27 151
PUMP	501 093
EVA-D	36 252
TURB	459 860
COND-D	34 315

7.5 Economic Analysis

After the exergy-cost analysis, an economic evaluation of the system is performed to estimate the exergo-economic cost of each stream defined as the product cost in monetary term. Two contributions are identified: the monetary cost of the exergy entering the plant to produce each stream and product within the plant and the remaining cost generated in the productive process associated with the achievement of product.

For a generic component the cost balance equation is written.

$$\sum_{i=1}^{n_{in}} c_{in,i} \cdot E_{in,i} + z = \sum_{i=1}^{n_{out}} c_{out,i} \cdot E_{out,i} \tag{38}$$

Where:

- c is the unit cost, in the case of monetary costs it is defined as the ratio between the cost C and the exergy E associated with the i stream.

$$c_i = \frac{C_i}{E_i} \tag{39}$$

- $\sum_{i=1}^{n_{in}} c_{in,i} \cdot E_{in,i}$ is the cost of the inlet streams.
- $\sum_{i=1}^{n_{out}} c_{out,i} \cdot E_{out,i}$ is the cost of the outlet streams.
- z is the cost of each component considering its availability, that is the annual percentage of operational hour. It is calculated for each component.

$$z = \frac{PV}{h_y \cdot 3600 \cdot AF} \tag{40}$$

Where:

- PV is the acronym for Present Value.
- h_y is the annual number of hours equal to 8760 h.
- $3600\ \frac{s}{h}$ is the conversion value from hours to seconds.
- AF is the acronym for Availability Factor, it is estimated as the ratio between the operating hours of the plant over the total annual hours. In the analysed plant it is assumed, for simplicity, to be the same for both charging and discharging phase, equal to 0,25. The annual working hours are then 2190 h.

The Equation 38, valid for the single component, can be written in a matrix form to consider the whole system.

$$A \times C = -Z \qquad (41)$$

Where:

- A is the $(n \times m)$ incidence matrix, reported in Table 1.
- C is the $(m \times 1)$ cost vector defined for each stream.
- Z is the $(n \times 1)$ vector containing all the cost rates for each component using Formula 40. The results obtained are reported in Table 24.

Table 24. Cost rates of components vector

	Z [$/s]
COMPR	24,01
HXW-C	25,01
VALVE	25,01
HXI-C	23,98
PUMP	40,37
HXW-D	41,37
TURB	45,15
HXR-D	40,37

As for the exergy cost analysis $m - n$ auxiliary equations are needed to find the exergo-economic cost for each stream. It is possible to use the same propositions with some

modifications for the external resources. In particular the exergo-economic cost of inlet streams to the system is considered equal to their price.

It is possible to redefine the matrix form, specified in Formula 38, adding the auxiliary equations obtained from P1, P2, P3 and P4 rules.

$$A_c \times C = Z_e$$
$$\begin{bmatrix} A \\ \alpha_e \\ \alpha_x \end{bmatrix} \times C = \begin{bmatrix} -Z \\ C_e \\ 0 \end{bmatrix} \quad (42)$$

Where:

- A_c is the $(m \times m)$ cost matrix that contains the incidence matrix A, the matrix α_e related to the P1 and P2 rules and the matrix α_x related to the P3 and P4 rules, reported in Table 9.
- C is the $(m \times 1)$ cost vector of the different streams.
- Z_e is the $(m \times 1)$ cost rates vector that contains the cost rates for each component Z, the cost of resources C_e related to preposition P1 and the cost of both flows discharged into the ambient (preposition P2) and non-exhausted fuel flows (preposition P3) both assumed to be null.

The resources cost vector C_e is assessed considering the exergo-economic cost of the energy and mass streams entering the control volume equal to its cost. The streams entering to the plant are the ones described by the auxiliary equation P1. The cost of the energy streams associated with the heat exchangers is null because the energy required is furnished by the working fluid on the other side of the heat exchanger, outside the considered CV. Instead, the cost of the energy streams associated with compressor and pump is estimated considering the electricity cost in different periods of time. The charge cycle is used in off-peaks hours, when the electricity production is higher than the demand and so the electricity cost is low. On the other hand, the discharge cycle is used in peaks hours, when the demand for electricity is higher than the production and so the electricity cost is high. The electricity cost in off-peak hours and peak hours for each month of the year 2022 is reported in Figures 6 and 7.

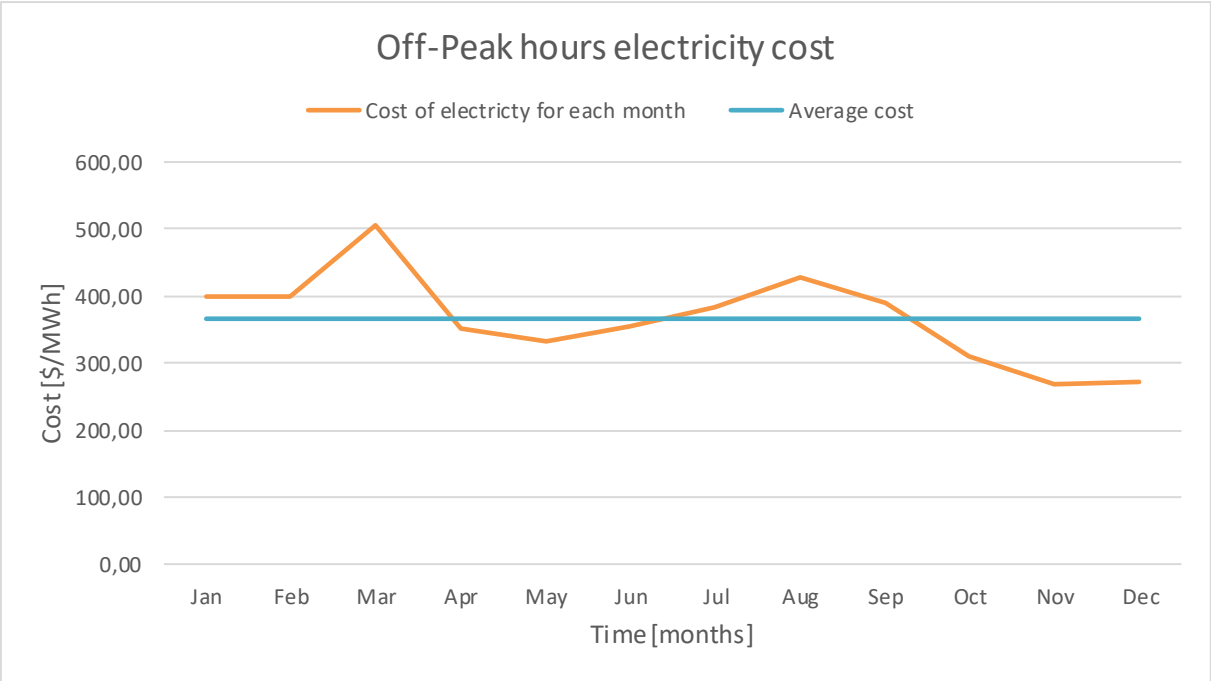

Figure 6. Off-peak hours electricity cost for Spain in 2022

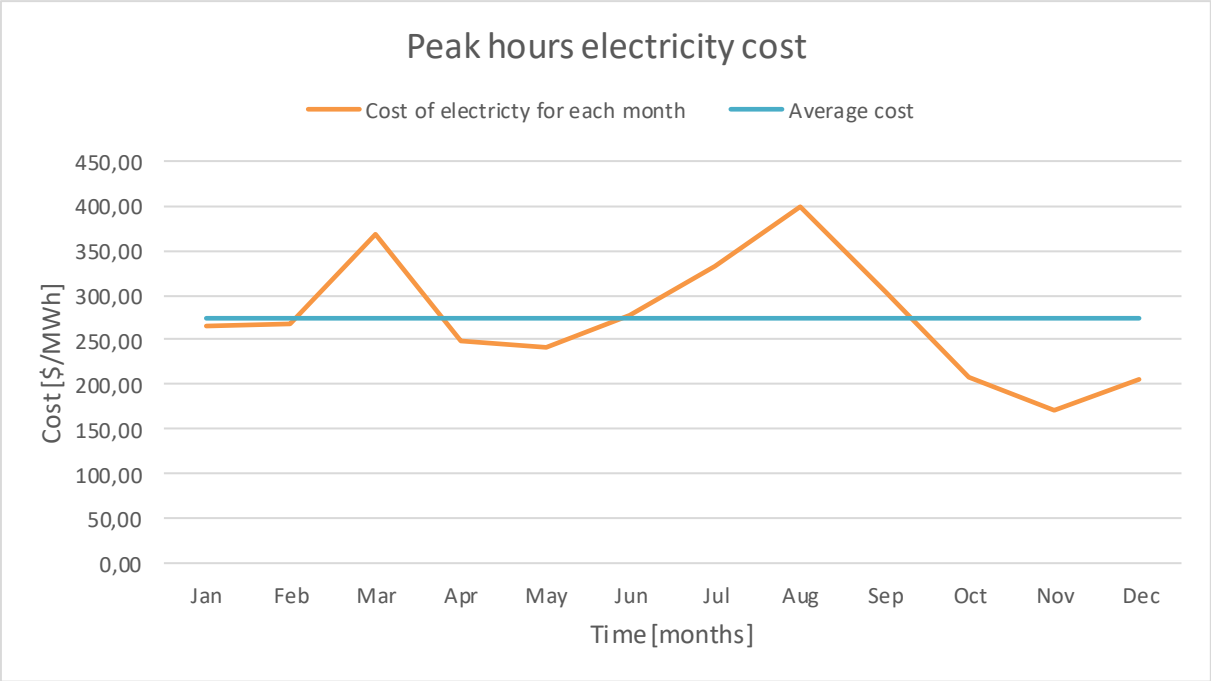

Figure 7. Peak hours electricity cost for Spain in 2022

From the Figures 6 and 7 the yearly average costs for both off-peak and peak electricity cost is underlined and reported below.

$$c_{el,off-peak} = 274{,}09\ \$/MWh$$

$$c_{el,peak} = 366{,}12\ \$/MWh$$

The cost of the energy streams associated with compressor and pump is then estimated. For the compressor is used the yearly average off-peak electricity cost and for the pump the peak one.

$$c = \frac{W \cdot AF \cdot c_{el}}{3600} \qquad (43)$$

Where:

- W is the power required by the specific component, compressor or pump.
- AF is the availability factor.
- c_{el} is the yearly average cost of electricity, off-peak or peak one.
- $3600\ \frac{s}{h}$ is the conversion value from hours to seconds.

The vector C_e is calculated using Formula 43 for the estimation of the energy stream cost for the compressor and the pump and setting equal to zero the energy stream cost for the heat exchangers. It is reported in Table 25.

Table 25. Resources cost vector

	Ce [$/s]
P1-COMPR	0,019
P1-PUMP	0,026
P1-EVA-D	0,000
P1-COND-D	0,000

Obtained the cost rates of components vector Z, reported in Table 24, and the resources cost vector C_e, reported in Table 25, it is possible to determine the cost rates vector Z_e, according to its definition expressed in Formula 42.

Table 26. Cost rates vector

Ze [$/s]	
COMPR	-0,022
COND-C	-0,004
VALVE	0,000
EVA-C	-0,003
PUMP	-0,064
EVA-D	-0,005
TURB	-0,058
COND-D	-0,004
P1	0,019
P1	0,026
P1	0,000
P1	0,000
P3	0,000
P3	0,000
P3	0,000

With the inverse of the matrix form expressed in Formula 42 it is possible to obtain the cost vector of the streams. It is reported in Table 27.

$$C = A_c^{-1} \times Z_e$$

Starting from the results in $\$/s$, the cost for a unit of energy for each stream is obtained using Formula 39. The obtained vector is reported in Table 28.

Table 27. Cost vector

C [$/s]	
1	0,52
2	0,56
3	0,53
4	0,53
5	0,80
6	0,89
7	0,90
8	0,80
W-COMPR	0,02
W-PUMP	0,03
W-TURB	0,16
Φ-COND-C	0,04
Φ-EVA-C	-0,01
Φ-EVA-D	0,00
Φ-COND-D	0,00

Table 28. Unit cost vector

c [$/MWh]	
1	309,92
2	290,72
3	290,72
4	309,92
5	86,02
6	93,20
7	87,68
8	87,68
W-COMPR	68,52
W-PUMP	91,53
W-TURB	158,74
Φ-COND-C	379,04
Φ-EVA-C	691,08
Φ-EVA-D	0,00
Φ-COND-D	0,00

8. Economic Indicators

The economic assessment of investment projects in the energy sector can be based on different methods. Discounted Cash Flow (DCF) methods are the most diffused and all of them rely on some considerations.

- The rate of return of the investment should be higher than a threshold level called hurdle rate that is fixed by the investor.
- The higher the risk, the higher the expected rate of return.
- The threshold level must reflect the financial combination adopted to finance the investment.
- Revenues should be evaluated basing on cash flows originated over the whole lifetime of the project.

To assess the economic feasibility of the analysed system some economic indicators are calculated.

8.1 Total Capital Expenditure of the plant

The Total Capital Expenditure (CAPEX) of the plant is estimated by summing all the TASC, reported in Table 21, for each component.

$$CAPEX = \sum_{i}^{N} TASC_i \qquad (44)$$

According to the Formula 44, the CAPEX is equal to $20\ 036\ 379\ \$$.

8.2 Total Operational Cost of the plant

The Total Operational Cost (OPEX) of the plant is related to the inlet energy and mass streams. Therefore, it takes into account only the cost related to the energy streams of the compressor and the pump considering that the energy required by the heat exchangers is furnished by the fluid on the other side. The Total Operational Cost is related to yearly basis.

$$OPEX = AF \cdot 8760\ h \cdot \left(W_{COMPR} \cdot c_{el,off-peak} + W_{PUMP} \cdot c_{el,peak}\right) \quad (45)$$

According to the Formula 45, the OPEX is equal to $1\ 414\ 166\ \$/y$.

8.3 Net Present Value

The Net Present Value (NPV) is the capability to estimate the investment of the plant, giving as result the amount of money that the plant is able to generate at the end of the lifetime. An investment project is accepted once the $NPV \geq 0$.

$$NPV = -I + \sum_{t=1}^{n} \frac{B_t}{(i+1)^t} \quad (46)$$

Where:

- I is the investment cost, equal to the CAPEX.
- n is the lifetime of the plant.
- i is the real discount rate, considered equal to the WACC.
- B_t is the annual cash flow over the whole lifetime of the project.

$$B_t = Incomes - Opex = Retail\ price \cdot E_{gen} - Opex \quad (47)$$

Where:

- E_{gen} is the energy produced by the turbine, estimated knowing the power produced W_{TURB} and the availability factor AF.

$$E_{gen} = W_{TURB} \cdot AF \cdot 8760\ h \qquad (48)$$

- $Retail\ price$ is the price at which the electricity produced is sold in the market. It is assumed equal to the average electricity cost in peak hours.

$$Retail\ price = 366{,}12\ \$/MWh$$

In Figure 8, the NPV trend over the whole lifetime of the plant is shown.

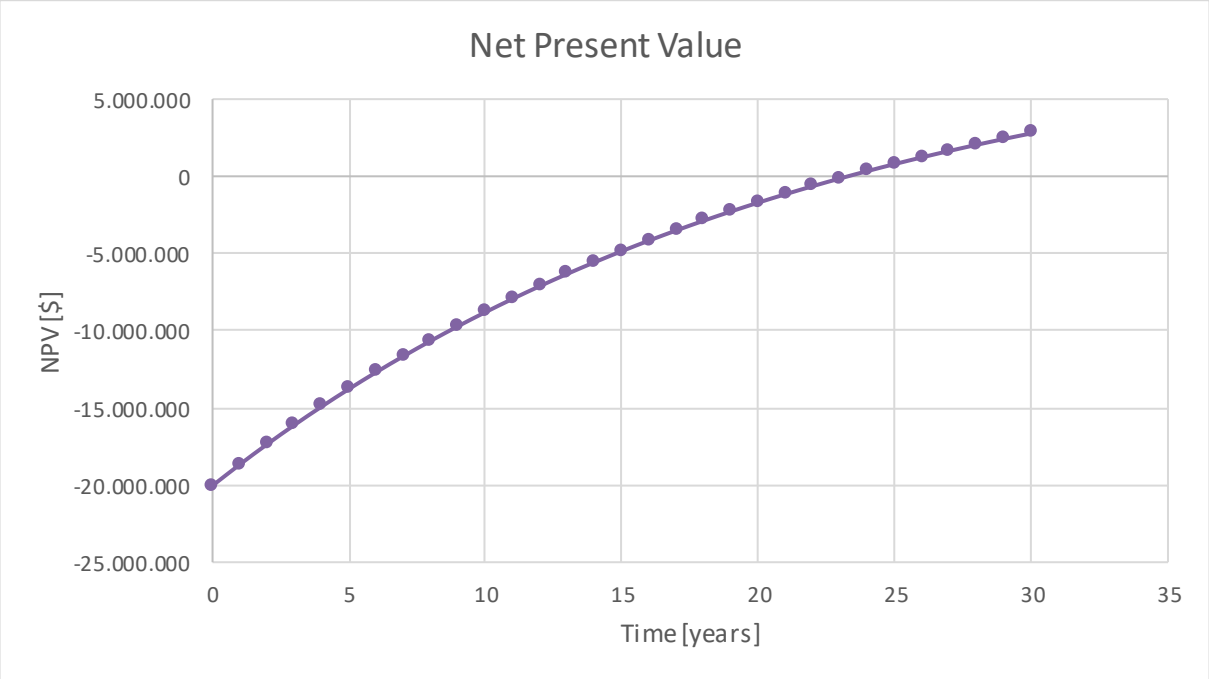

Figure 8. Net Present Value trend over the lifetime of the plant for the year 2022

Usually, the economic performance of TES is limited with a Payback Time, corresponding to a positive NPV, of always over 7 years [34]. Considering that the analysed plant is more complex than a basic TES and it is integrated with an electricity production system it is reasonable to obtain a higher value for the Payback Time than the expected one.

8.4 Other economic indicators

The Benefit Cost Ratio (BCR) describes the average profitability of an investment per unit of invested capital.

$$BCR = \frac{\sum_{t=1}^{n} \frac{B_t}{(i+1)^t}}{I} \tag{49}$$

The Internal Rate of Return (IRR) is the value of the discounted rate i that makes the sum of discounted cash flow equal to the investment cost.

$$-I + \sum_{t=1}^{n} \frac{B_t}{(IRR+1)^t} = 0 \tag{50}$$

The Payback Time (PBT), expressed in years, measures the time when the NPV becomes positive.

$$-I + \sum_{t=1}^{n} \frac{B_t}{(i+1)^t} = 0 \tag{51}$$

The Levelized Cost of Energy (LCOE) is the price of electricity that leads to have $NPV = 0$

$$LCOE = \frac{CAPEX + \sum_{t=1}^{n} OPEX_t \cdot (i+1)^{-t}}{\sum_{t=1}^{n} E_{gen,t} \cdot (i+1)^{-t}} \tag{52}$$

In Table 29 the results for the economic indicators defined above are reported.

Table 29. Values of the economic indicators

BCR [-]	IRR [%]	PBT [y]	LCOE [$/MWh]
1,14	5,86	24	343,64

9. Sensitivity Analysis

A sensitivity analysis is performed changing some selected parameters in a precise range, usually $\pm 10\%$, and observing the effect on the NPV trend. For the analysed system the selected parameters are the AF, the electricity cost during off-peaks hours and the retail price of electricity. In Tables 30, 31 and 32 the ranges of change for each parameter and the corresponding variation of NPV are reported.

Table 30. Sensitivity analysis to the retail price

Range	Retail price [$]	NPV [$]	Variation NPV
-10%	329,51	-1 748 788	-163%
0%	366,12	2 783 191	0%
10%	402,73	7 315 170	163%

Table 31. Sensitivity analysis to the availability

Range	Availability [%]	NPV [$]	Variation NPV
-10%	0,23	957 625	-66%
0%	0,25	2 783 191	0%
10%	0,27	4 608 757	66%

Table 32. Sensitivity analysis to the electricity cost

Range	Electricity cost [$]	NPV [$]	Variation NPV
-10%	246,69	3 738 372	34%
0%	274,09	2 783 191	0%
10%	301,50	1 828 160	-34%

The results obtained for the sensitivity analysis are shown in Figure 9 using a Spider Diagram. The slopes of the curves highlight in which ways the NPV trend is affected by the change of the selected parameters. In particular, the NPV is more affected by the change of the retail price.

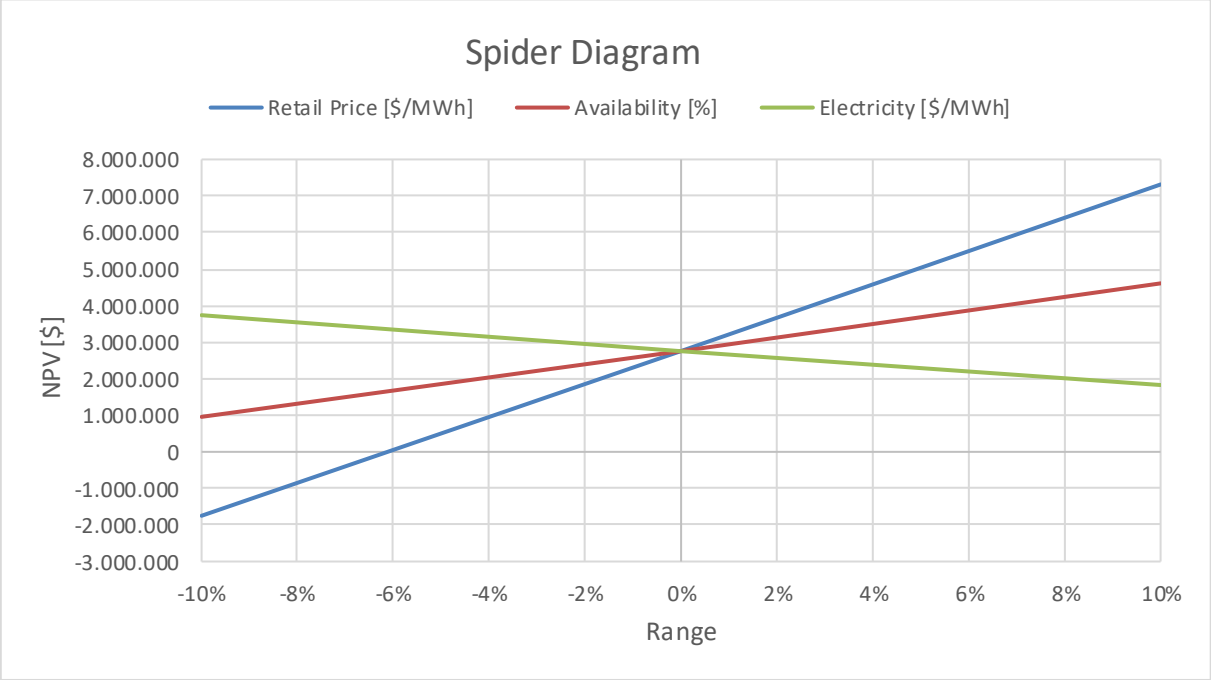

Figure 9. Spider Diagram resulting from the sensitivity analysis

10. 2023 scenario analysis

The exergo-economic analysis is previously performed for the year 2022 but, due to various factors, such as the European energy shortage, the electricity cost is increased by 88% as compared to the average for the years antecedents [35]. The Government of Spain has taken measures to counteract, though not entirely stop, the increase in electricity cost. Among these measures are the approval of the electricity decree in 2022 with the RDL 18/2022, which includes bill VAT rebates, social bonus extensions, and electricity tax reductions; the Iberian exception, which sets a cap on the price of gas for electricity generation; and subsidies for self-consumption and renewable energy. Starting from this specific scenario so, a different and a more actual one, is analysed considering the year 2023. In Table 33 the average electricity cost and the CEPCI for both the years are reported.

Table 33. Comparison between electricity cost and CEPCI

	2022	*2023*
Electricity cost [$/MWh]	302,32	156,81
CEPCI [-]	815,98	797,94

In Figures 10 and 11 are reported the electricity cost in off-peak hours and peak hours for each month of the year 2023 and the averages for the whole year. Comparing to the year 2022 a decrease in both the trends is highlighted. As reported in Tables 30 and 32, the NPV is affected by the variation of the electricity cost in off-peak hours and peak hours. The expectation is for the NPV trend to strongly decrease due to the decrease of the retail price, considered equal to the average electricity cost in peak hours.

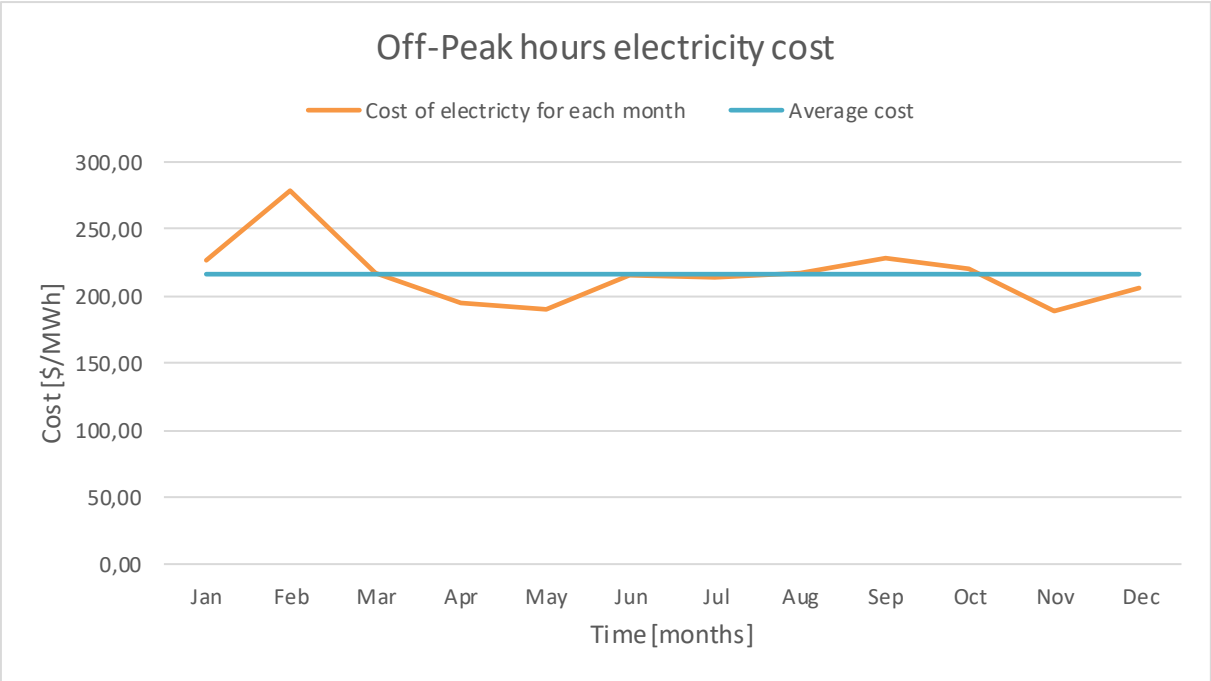

Figure 10. Off-peak hours electricity cost for Spain in 2023

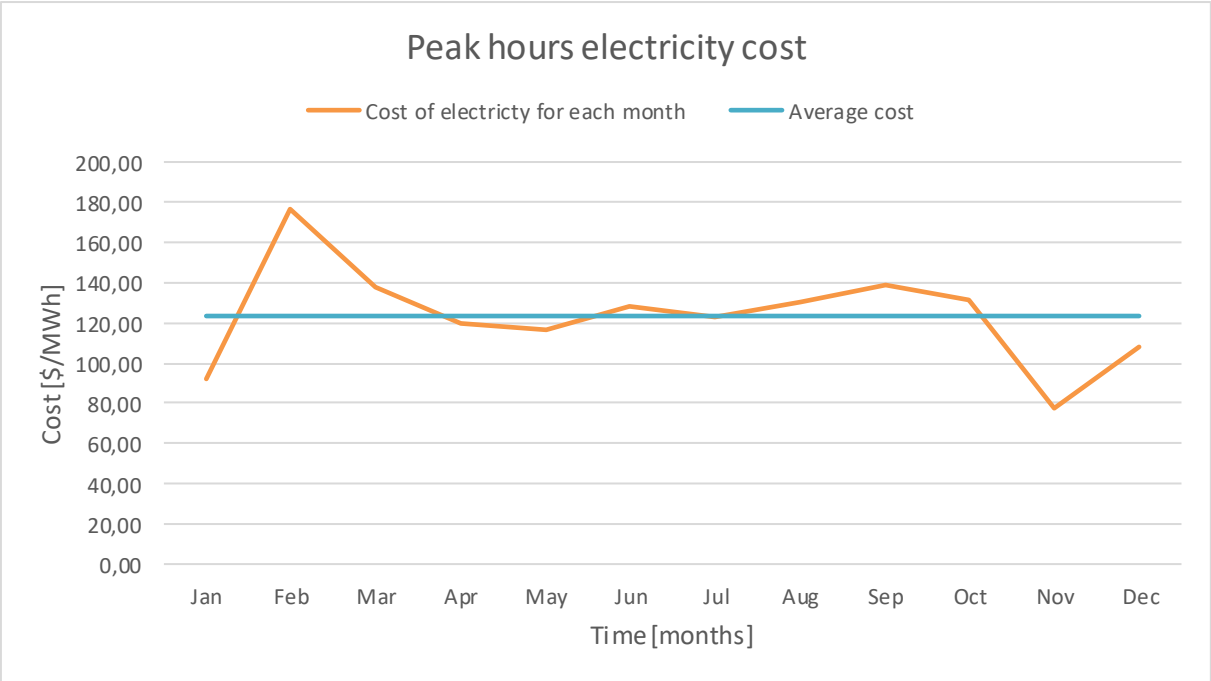

Figure 11. Peak hours electricity cost for Spain in 2023

Varying only the CEPCI and the electricity cost for off-peaks and peaks hours, the trend of the NPV changes dramatically as expected. In fact, it never reaches a positive value for the estimated lifetime of the plant as shown in Figure 12.

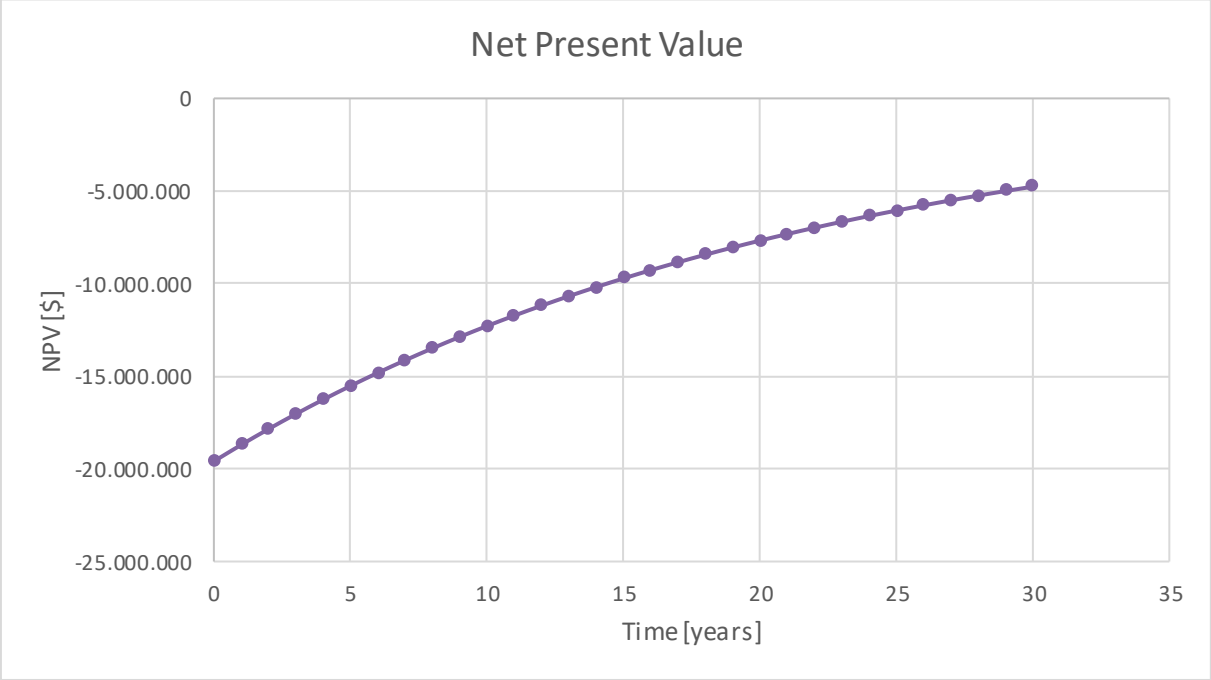

Figure 12. Net Present Value trend over the lifetime of the plant for the year 2023

11. Integration scenarios for the reference system

In this section different integration scenarios are considered to increase the performance of the reference system. Starting from [2] where an open cycle configuration paired with geological storage is presented and analysed, other configurations are proposed to match with the reference system and to solve some technical problems highlighted by the modelling part.

11.1 Open cycle system

CO_2 capture and geological disposal is considered one of the most promising technologies to mitigate atmospheric emissions, produced by large-scale fossil fuel usage for power production and industries, and climate changes. Different technologies are available for capturing the carbon dioxide such as pre-combustion, post-combustion and oxy-fuel combustion carbon capture. Currently most of these technologies allows an absorption nearly equal to 85-95% of the CO_2 produced by a power plant. After the capture the CO_2 must be transported with pipelines, in supercritical condition, to the geological storage [36].

Among the different CO_2 storage options, geological formations are the cheapest and most environmentally acceptable option [37]. There are a lot of different potential geological reservoirs, already used in the past to store oil and gas, such as depleted and disused oil and gas fields, deep saline aquifers and deep unminable coal seams [38]. All these sites have been selected because they present an adequate storage capacity, injectivity, good confining unit or sealing caprock, and a stable geological environment to prevent compromising the site.

The geological storage system includes two wells: the primary well (W-A) and the secondary well (W-B). The primary well is linked to the energy production pressure and the extraction temperature, which is influenced by the well's depth. A portion of the CO2 injected into the secondary well migrates out of the geological reservoir and becomes permanently sequestered in the geological formation. The remaining CO2 moves to the primary well due to the thermosiphon effect, where the fluid heats up, expands, and decreases in density. This

CO2 is heated throughout the process and is recovered during the subsequent discharge phase. To achieve the thermosiphon effect, wellhead pressure values of 5–6 MPa and temperatures of 10–20 °C are required.

In Figure 13 is reported the working scheme of the open HP (0-4-1-2-3-A) and the open HE (A-6-7-8-5-B). During energy excess production, the plant receives supercritical CO_2 from a carbon capture facility and it converts the electrical energy into thermal one, storing sensible heat in the condenser at HT and using latent heat in the evaporator at LT. After the condenser, the CO_2 is transported with pipelines to the storage site, ideally a local geological storage is considered, and injected into W-A. During energy deficit production, the CO_2 is extracted from W-A of the geological storage and the thermal energy is converted into electrical one using the sensible heat in the evaporator at HT and releasing latent heat in the condenser at LT. After the condenser, the CO_2 is injected into W-B, located hundreds of meters from W-A, but in the same geological reservoir, with lower pressure and temperature comparing to its extraction. The theoretical cycle uses latent heat in the LT side to evaporate or to condense the CO_2 but, in the reference system, sensible heat is used due to impossibility of the modelling software, Aspen Hysys®, to work with solid material in the heat exchangers.

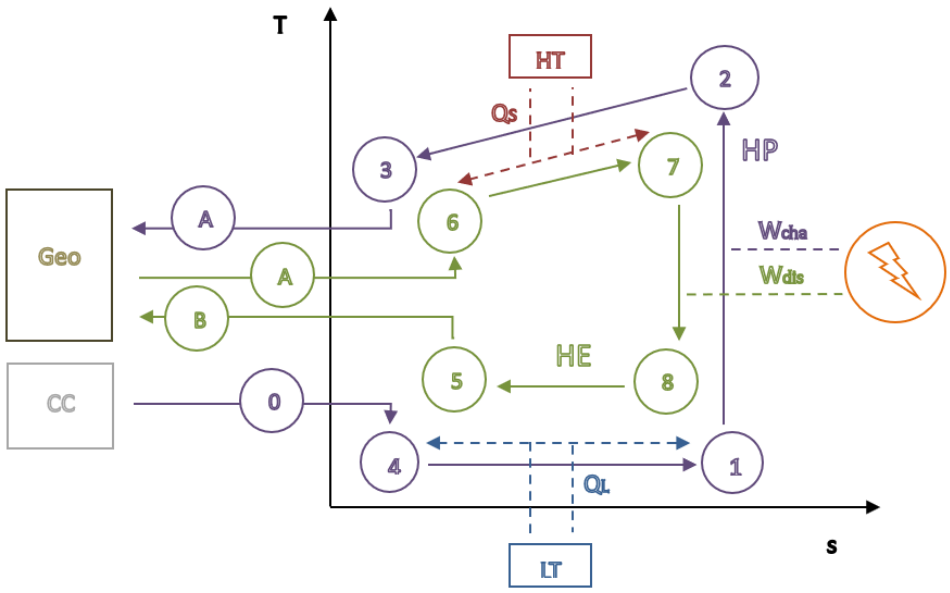

Figure 13. Reversible heat pump energy storage system with well-integrated temperature profile, including geological storage

11.1.1 Aspen Hysys® modelling

In Figure 14 is reported the scheme of the open cycle in charge and discharge operation with all the components and the streams. The charge open cycle is located at the left of the scheme while the discharge open cycle on the right.

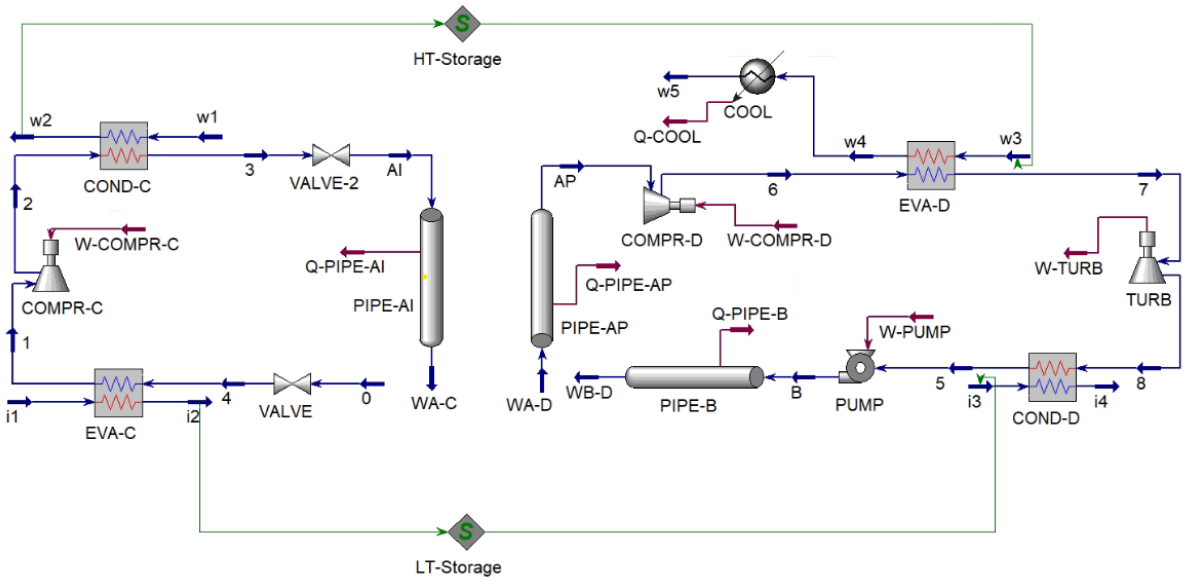

Figure 14. Scheme of the open cycle paired with geological storage and carbon capture

The charge open cycle is composed of the following components:

- *VALVE - Valve:* it expands the CO_2 to reach the low-pressure level of the cycle. At the exit the fluid is constituted by a vapour and a liquid phase.
- *EVA-C - Evaporator*: it evaporates the CO_2 until reaching the saturation condition. The H_2O enters the hot side of heat exchanger and releases sensible heat to the CO_2. Then it is stored in a LT tank to be used in the discharge cycle.
- *COMPR-C - Compressor:* it compresses the CO_2 coming from the evaporator increasing the pressure and the temperature values to reach the high-pressure level of the cycle.
- *COND-C - Condenser*: it condenses the hot CO_2 exchanging heat with the H_2O. The H_2O enters the cold side of the heat exchanger receiving the heat released from the CO_2. At the end it is stored in a HT tank to be used in the discharge cycle.
- *VALVE-2 - Valve*: it expands the CO_2 to reach the required pressure level and temperature for the injection in the geological storage.

- *PIPE-AI - Pipe*: it simulates the injection of the CO_2 into W-A considering the heat exchange with the ground. It is stored to be used in the discharge cycle.

The discharge open cycle is composed of the following components:

- *PIPE-AP - Pipe:* it simulates the extraction of the CO_2 from W-A considering the heat exchange with the ground to reach the required pressure level and temperature. At the exit the fluid is constituted by a vapour phase.
- *COMPR-D - Compressor:* it increases the pressure and the temperature of the CO_2 to reach the high-pressure level of the cycle.
- *EVA-D - Evaporator*: it increases the temperature of the CO_2 absorbing the heat released by the H_2O. The H_2O comes from the HT tank, and it enters the hot side of the heat exchanger. At the end it is released in the environment.
- *COOL - Cooler*: it decreases the temperature of the H_2O before releasing it to the environment.
- *TURB - Turbine*: it expands the CO_2 to reach the low-pressure level of the cycle.
- *COND-D - Condenser*: it condenses the CO_2 to the saturation condition releasing heat to the H_2O. In fact, the H_2O coming from the LT storage, enters the cold side of the heat exchanger and it is heated up.
- *PUMP - Pump*: it increases the pressure and the temperature of the CO_2, coming from the condenser, to reach the required pressure level for the injection in the geological storage.
- *PIPE-B - Pipe*: it simulates the injection of the CO_2 into W-B considering the heat exchange with the ground.

The CO_2 collected from a carbon capture plant is conveyed through pipelines and can be stored in either a geological formation or a steel tank to minimize supply fluctuations and optimize the integration of renewable energy. Steel tanks can hold up to 3000 tons of pressurized CO_2. It is assumed that the conditions of CO_2 within the steel tank and at point 0 are identical to those during transportation from the carbon capture plant: high pressure and ambient temperature. For optimal plant performance and efficient loading and unloading, CO_2 should be maintained in a liquid or supercritical dense phase.

The main difference between the modelling of the close cycle and the open one is the presence of the pipes. This component simulates the injection in the geological storage located at 1800 m underground. It is divided in 6 segments with the length of 300 m each and it transfers heat with the CO_2 contained inside and the ground. For the heat exchange with the ground a geothermal gradient equal to 2-3 °C/100 m is considered.

The system is constructed adding all the components explained before and inserting the input parameters that are summarized in Table 35 and 36. [39]

Table 34. Main assumptions, inputs and hypothesis on the modelling of the open charge cycle

Input parameters open charge cycle

VALVE	Inlet Pressure	100	bar
	Inlet Temperature	12	°C
	Outlet Pressure	30	bar
EVA-C	Min Approach Temperature	4	°C
	Pressure Drop	0	bar
	Inlet Temperature Hot Side	10	°C
	Inlet Pressure Hot Side	5	bar
COMPR-C	Isentropic Efficiency	0,86	-
	Inlet Vapor fraction	1	-
	Power	1	MW
	Outlet Pressure	200	bar
COND-C	Min Approach Temperature	4	°C
	Pressure Drop	0	bar
	Inlet Temperature Cold Side	25	°C
	Inlet Pressure Cold Side	12	bar
VALVE-2	Outlet Pressure	90	bar
PIPE-AI	Depth of the reservoir	1800	m
	Outer diameter	140	mm
	Inner diameter	90	mm

Table 35. Main assumptions, inputs and hypothesis on the modelling of the open discharge cycle

Input parameters open discharge cycle

PIPE-AP	Depth of the reservoir	1800	m
	Outer diameter	140	mm
	Inner diameter	90	mm
COMPR-D	Inlet Temperature	37,6	°C
	Inlet Pressure	83,4	bar
	Isentropic Efficiency	0,86	-
	Power	1	MW
	Outlet Pressure	200	bar
EVA-D	Min Approach Temperature	4	°C
	Pressure Drop	0	bar
	Inlet Temperature Hot Side	134,9	°C
	Outlet Temperature Hot Side	91	°C
	Inlet Pressure Hot Side	12	bar
COOL	Outlet Temperature	25	°C
	Pressure Drop	0	bar
TURB	Isentropic Efficiency	0,88	-
	Outlet Pressure	40	bar
COND-D	Min Approach Temperature	4	°C
	Pressure Drop	0	bar
	Inlet Temperature Cold Side	-1,046	°C
	Inlet Pressure Cold Side	5	bar
PUMP	Isentropic Efficiency	0,85	-
	Inlet Liquid fraction	1	-
	Outlet Pressure	90	bar
PIPE-B	Depth of the reservoir	1800	m
	Outer diameter	140	mm
	Inner diameter	90	mm

The thermodynamic state at each point is obtained and the main output parameters are reported in Table 37.

Table 36. Thermodynamic state of the mass streams for the open cycle

Stream	*m [kg/s]*	*T [°C]*	*p [bar]*	*Vapour Fraction [-]*
0	9,525	12	100	0
4	9,525	-5,049	30	0,14
1	9,525	-5,048	30	1
2	9,525	165	200	1
3	9,525	29,07	200	0
AI	9,525	20,7	90	0
WA-C	9,525	39,21	233,6	0
w1	5,590	25	12	0
w2	5,590	139,4	12	0
i1	43,26	10	5	0
i2	43,26	-1,049	5	0
WA-D	32,01	92,61	258,3	0
AP	32,01	37,6	83,4	1
6	32,01	86,03	190	1
7	32,01	135,4	190	1
8	32,01	10,54	40	1
5	32,01	5,594	40	0
B	32,01	11,80	90	0
WB-D	32,01	25,47	202	0
w3	14,97	139,4	12	0
w4	14,97	91	12	0
w5	14,97	25	12	0
i3	604,7	-1,049	5	0
i4	604,7	1,693	5	0

As expected, comparing these results to the ones of the reference system, due to the mass flow rate decrease of the discharge cycle, equal to 32,01 kg/s, and the temperature decrease of the HT storage, equal to 139,4°C, the turbine power decreases to 1,920 MW. Moreover, the issue related to the high H_2O mass flow rate needed for the condenser of the discharge cycle is not solved with this configuration, as it is equal to 604,7 kg/s. Different scenarios based on latent heat exchange are presented for the low temperature part of the closed cycle to overcome this technical problem underlined by the modelling of both the closed and open cycle.

11.2 Low temperature integration

For the reference system H_2O is used to perform sensible heat exchange in the LT part of the charge and discharge cycle. In Figures 15 and 16 are reported the plots of the temperatures of hot and cold composites as function of the heat flux exchanged for both the charge and discharge cycle. As shown, the H_2O for both the evaporator and the condenser doesn't undergo a phase change and it performs only sensible heat exchange.

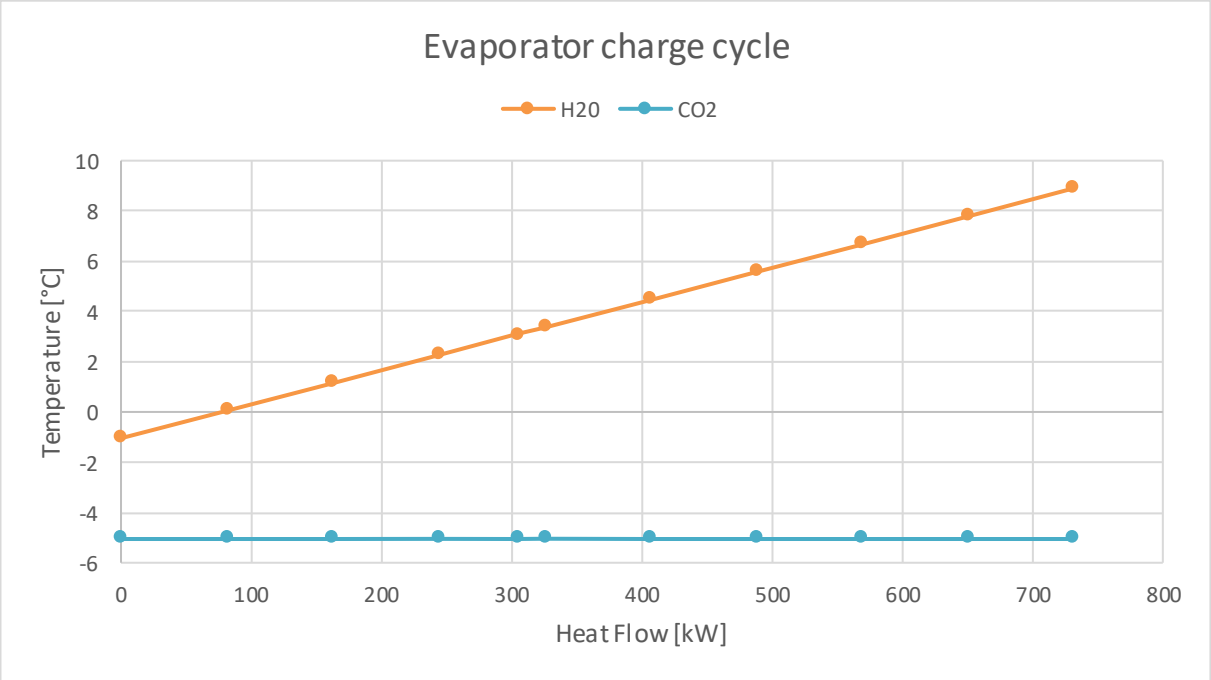

Figure 15. Trend of temperatures as function of heat flow for the evaporator of the charge cycle

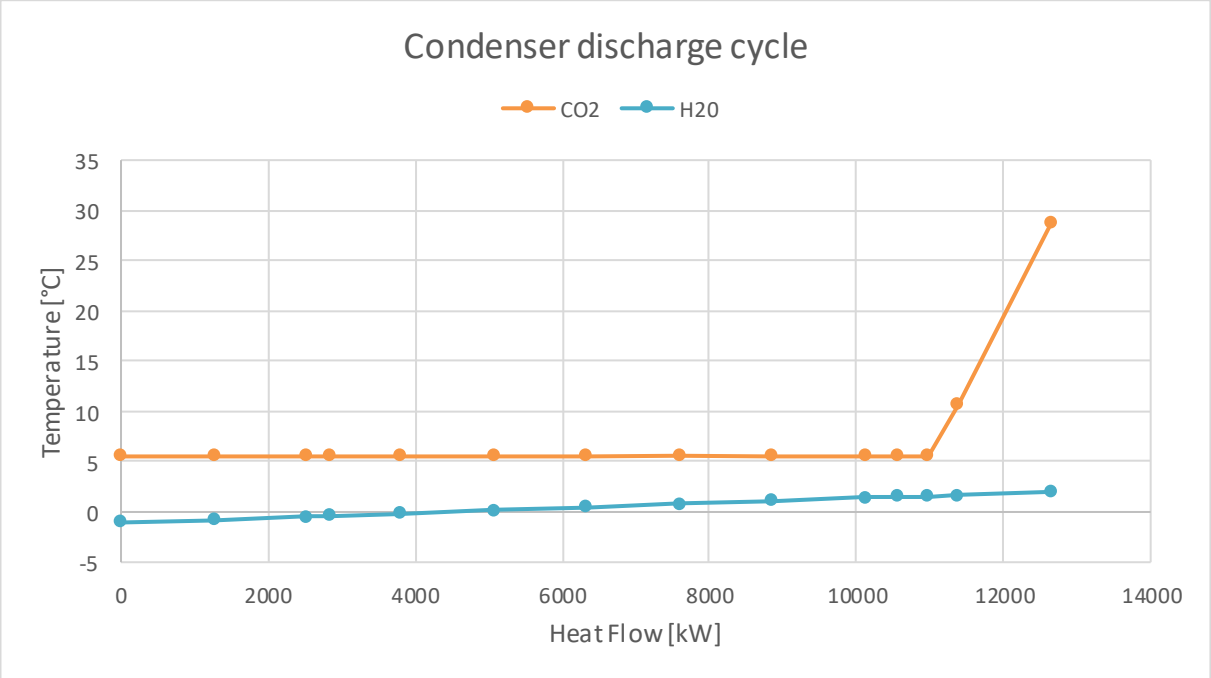

Figure 16. Trend of temperatures as function of heat flow for the condenser of the discharge cycle

The H_2O mass flow rate obtained in the reference system to perform the heat transfer in the discharge cycle is equal to 959,5 kg/s, as reported in Table 6, and it is not acceptable as a result. In order to obtain an acceptable output for this value and to increase the performance of the system itself different integration scenarios are proposed.

11.2.1 Refrigerants for latent heat exchange

For the heat exchange the most suitable materials are the refrigerants, substances or mixtures that are used in heat cycles and go through a phase transition from gas to liquid and vice-versa. Refrigerants are divided in five categories: chlorofluorocarbons (CFCs), hydrochlorofluorocarbons (HCFCs), hydrofluorocarbons (HFCs), natural refrigerants and refrigerant blends (zeotropic blends and azeotropic blends) [40]. Even if technological and economic development have helped refrigeration system gain global attention, the emissions from refrigeration systems can affect the environment by raising the surface temperature of the earth and depleting the ozone layer. In particular the Global Warming Potential (GWP) of hydrofluorocarbons is very high as the Ozone Depletion Potential (ODP) of the chlorofluorocarbons. Another way to classify refrigerants is according to different generations each one related to a specific period of time [41].

The first generation of refrigerants (1830-1930s) was characterized by the use of whatever material worked and whatever was available. Almost all the first-generation refrigerants were flammable, toxic or both and some were also highly reactive. The most diffused ones and their properties are reported in Table 38.

Table 37. First generation of refrigerants and their properties

Substance	*R number*	*M [kg/kmol]*	*NBP [°C]*	*ODP*	*GWP*
Carbon dioxide	R-744	44,01	-55,6	0	1
Ammonia	R-717	17,03	-33,3	0	0
Sulphur dioxide	R-764	64,06	-10,0	0	0
Ethyl ether	R-610	74,12	35	0	0
Dimethyl ether	R-170	46,07	-25	0	0
Methyl chloride	R-40	50,49	-24,2	0,02	16

The second generation (1931-1990s) of refrigerants was characterized by a shift to chlorofluoro chemicals for safety and durability. In fact, CFCs refrigerants are non-toxic, non-reactive and non-flammable gas with relatively high mass. After discovering in 1970 that they break ozone molecules in oxygen molecules being harmful to the ozone layer, in 1987 with the Montreal Protocol their production and consumption was limited. The most diffused ones and their properties are reported in Table 39.

Table 38. Second generation of refrigerants and their properties

Substance	*R number*	*M [kg/kmol]*	*NBP [°C]*	*ODP*	*GWP*
Trichlorofluoro methane	R-11	137,4	23,71	1	4000
Dichloro difluoro methane	R-12	120,91	-29,75	1	8500
Chloro trifluoro mthane	R-13	104,5	-81,3	1	11700
Chloro difluoro methane	R-22	86,47	-40,8	0,055	1700

The third generation (1990-2010s) of refrigerants was characterized by low ODP. This included mainly HFCs that does not pose a risk to the ozone layer, but they contribute towards global warming. The Kigali Agremement in 2016 signalled the progressive phasing-out of these refrigerants. The most diffused ones and their properties are reported in Table 40.

Table 39. Third generation of refrigerants and their properties

Substance	*R number*	*M [kg/kmol]*	*NBP [°C]*	*ODP*	*GWP*
Difluoromethane	R-32	-52,02	-51,65	0	580
Tetrafluoroethane	R-134a	102,03	-26,07	0	1300
R-125 + R-143a + R-134a	R-404a	97,6	-46,6	0	3800
R-32 + R-125 + R-134a	R-407C	86,2	-43,8	0	1600
R-32 + R-125	R-410a	72,59	-51,6	0	1900

Nowadays the refrigerants that dominate the market are natural refrigerants because they are easily available and they present low values for ODP and GWP [42]. The most diffused ones and their properties are reported in Table 41. Carbon dioxide (CO_2) and ammonia (NH_3) can be also considered natural refrigerants and their properties are reported in Table 38.

Table 40. Natural refrigerants and their properties

Substance	*R number*	*M [kg/kmol]*	*NBP [°C]*	*ODP*	*GWP*
Propane	R-290	44,1	-42,1	0	3
Propene	R-1270	42,08	-47,7	0	1,8
Butane	R-600	58,12	-11,7	0	3
Isobutane	R-600a	58,12	-0,5	0	3

Due to the Montreal Protocol on Substances That Deplete the Ozone layer and the Kigali Amendment to the Montreal Protocol the only refrigerants that are considered for the simulations are the natural ones. The H_2O in the LT part of both the charge and discharge cycle is substituted, simulation after simulation, by the natural refrigerants reported in Table 38 and 41. The main idea is that these refrigerants, comparing to the reference system with H_2O, perform a latent heat exchange.

For the first simulation the refrigerant propane (R-290, C_3H_8) is used, which properties are reported in Table 41. In order to obtain a latent heat transfer the minimum approach temperature for the condenser of the discharge cycle is decreased to 3 °C, comparing to the reference system when it was 4 °C, as reported in Table 5. Considering this input, the H_2O mass flow rate in the discharge cycle remains a non-acceptable value, as it is equal to 696,2 kg/s. Using the refrigerant R-290 instead, a different and acceptable result for the mass flow rate in the discharge cycle is obtained as reported in Table 42.

Table 41. Results of the mass flow rate using R-290 for the charge and discharge cycle

$G_{R\text{-}290,C}$ [kg/s]	$G_{R\text{-}290,D}$ [kg/s]
2,06	30,03

In Figures 17 and 18 are reported the temperatures plots of hot and cold composites as function of the heat flux exchanged for both the charge and discharge cycle. As shown, the R-290 undergoes a phase change from vapour to liquid in the evaporator and vice versa in the condenser and performs latent and sensible heat exchange.

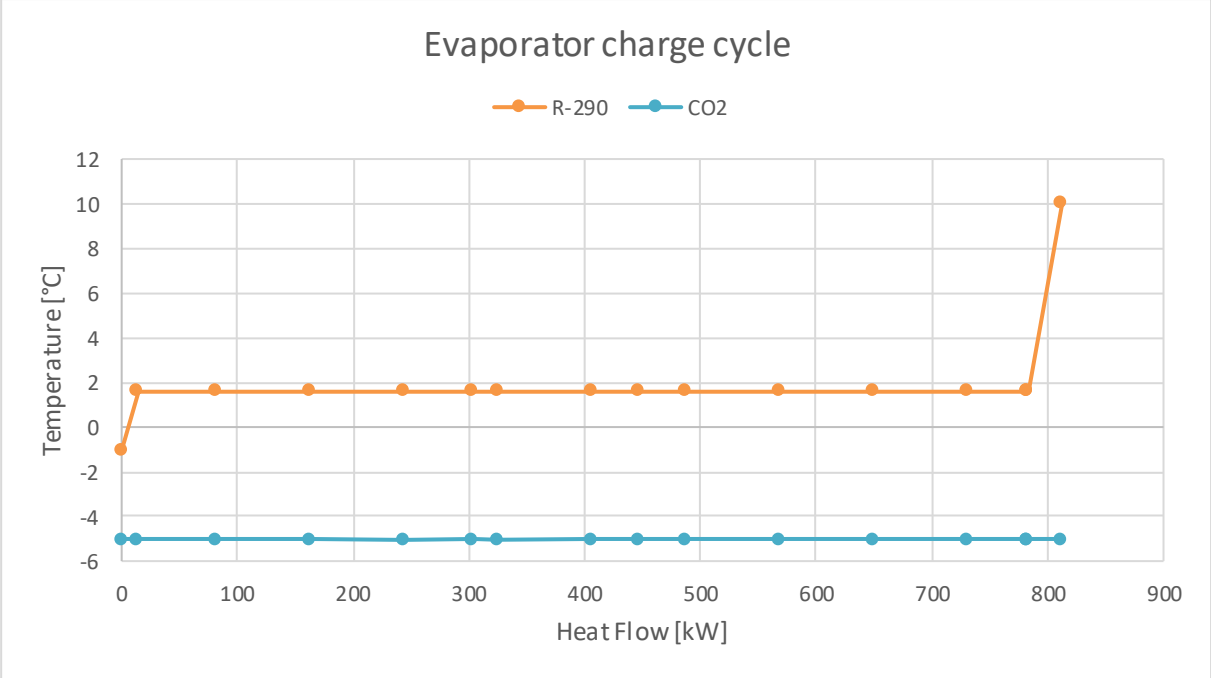

Figure 17. Trend of temperatures as function of heat flow for the evaporator of the charge cycle

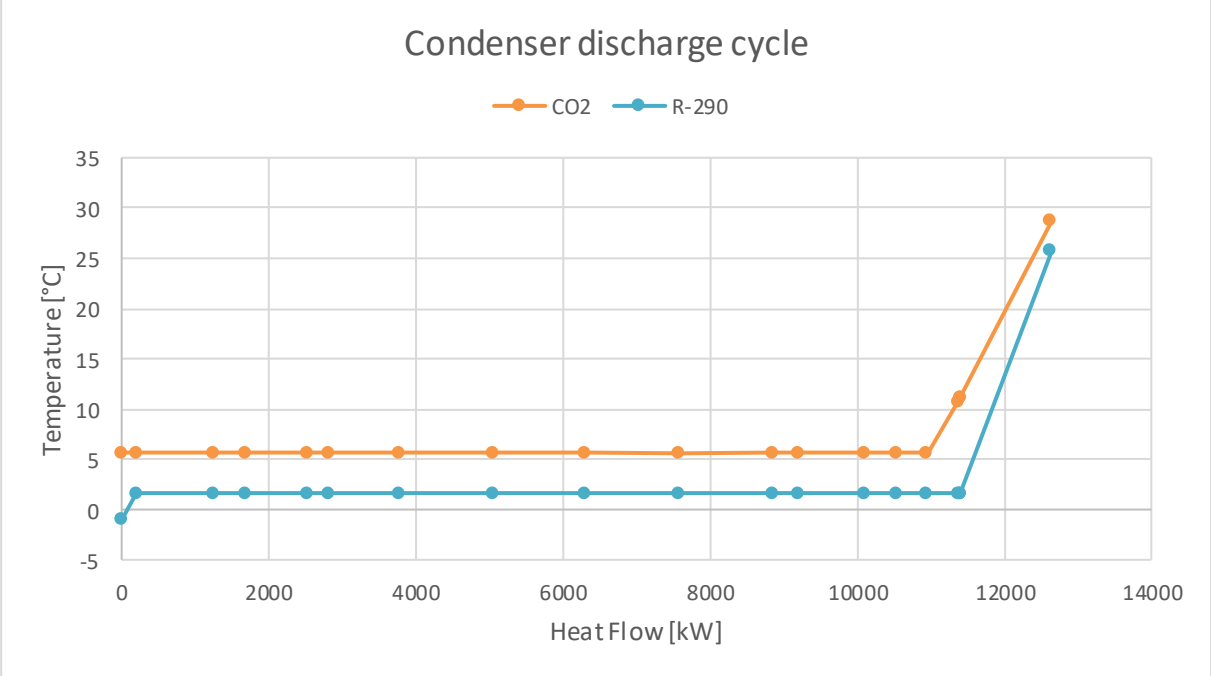

Figure 18. Trend of temperatures as function of heat flow for the condenser of the discharge cycle

The simulation is performed also with all the natural refrigerants reported in Table 41, but the different properties, in particular the NBP, make them not compatible with the temperatures that are required for the hot composite in the evaporator and the cold composite in the

condenser. The only other refrigerant that is possible to use is ammonia (R-717, NH_3), which properties are reported in Table 38. In order to obtain a latent heat transfer the minimum approach temperature for the condenser of the discharge cycle is decreased to 1 °C, comparing to the reference system when it was 4 °C, as reported in Table 5. Considering this input, the H_2O mass flow rate in the discharge cycle remains a non-acceptable value, as it is equal to 449,5 kg/s. Using the refrigerant R-717 instead, a different and acceptable result for the mass flow rate in the discharge cycle is obtained as reported in Table 43.

Table 42. Results of the mass flow rate using R-717 for the charge and discharge cycle

$G_{R\text{-}717,C}$ [kg/s]	$G_{R\text{-}717,D}$ [kg/s]
0,62	9,31

In Figures 19 and 20 are reported the plots of the temperatures of hot and cold composites as function of the heat flux exchanged for both the charge and discharge cycle. As shown, the R-717 undergoes a phase change from vapour to liquid in the evaporator and vice versa in the condenser and performs latent and sensible heat exchange.

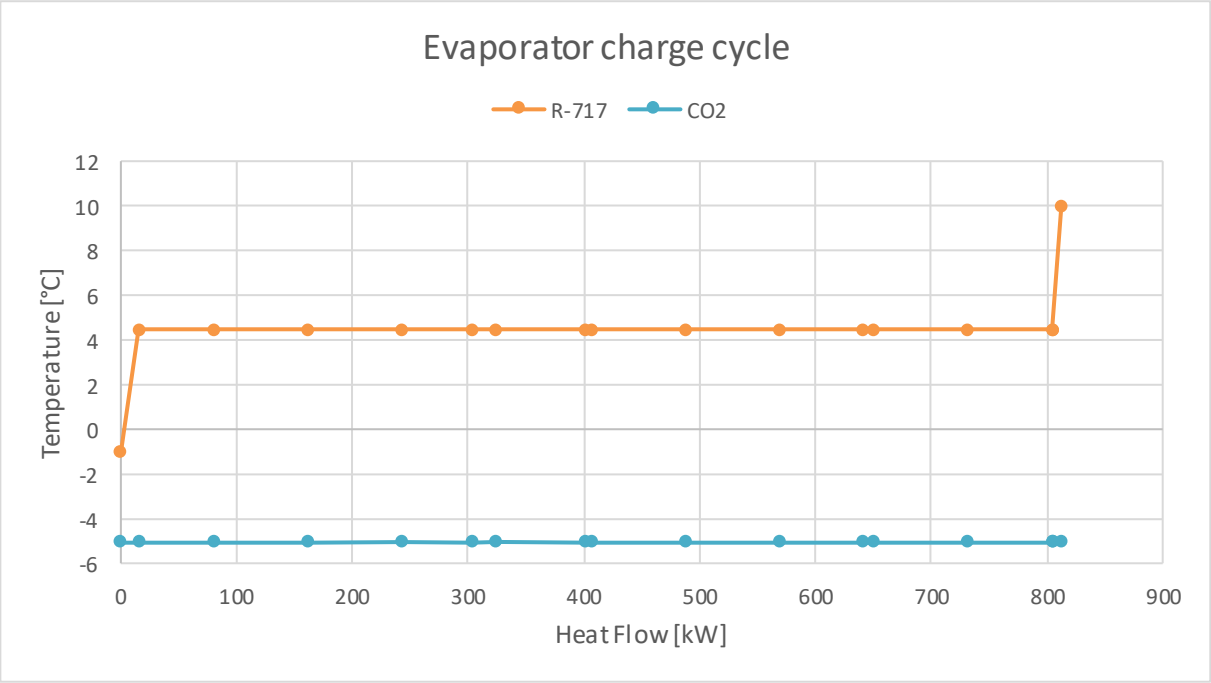

Figure 19. Trend of temperatures as function of heat flow for the evaporator of the charge cycle

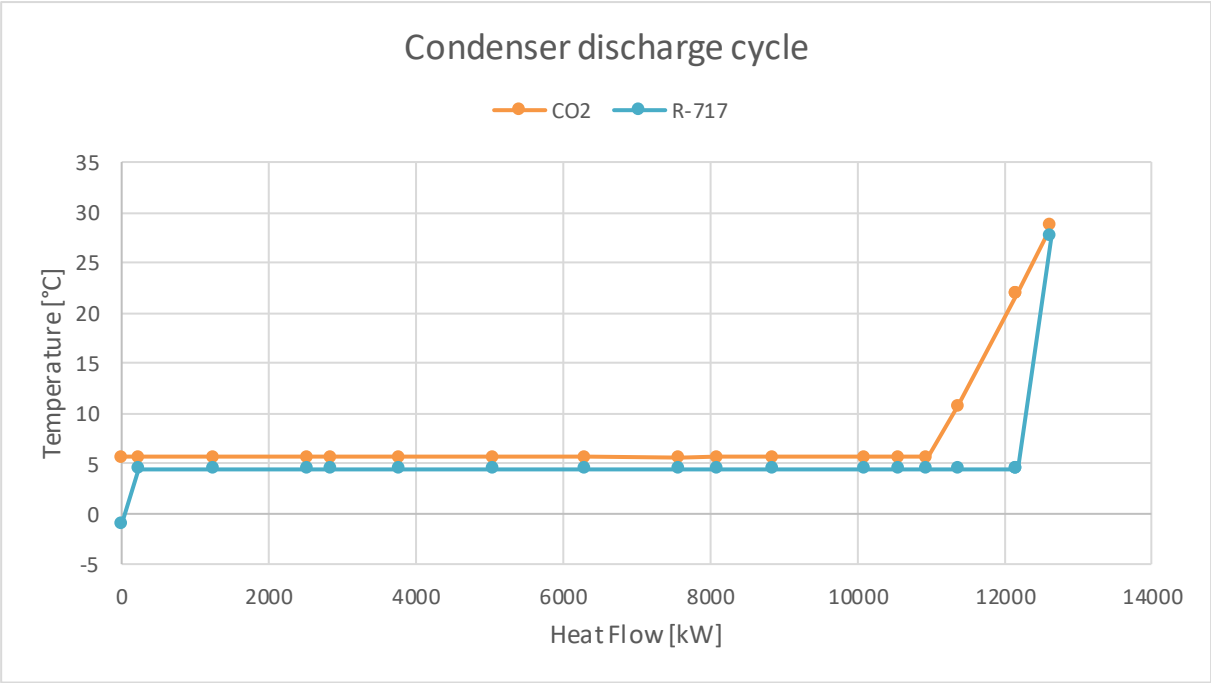

Figure 20. Trend of temperatures as function of heat flow for the condenser of the discharge cycle

In conclusion, the configuration that uses R-717 as refrigerant is the one that brings to lower values of the mass flow rate, due to the thermos-physical properties (low boiling point and high latent heat of vaporization) of this material. For this reason, another integration scenario that uses this refrigerant is considered and explained below.

11.2.2 Absorption chiller

An alternative refrigeration system that reduces the electricity consumption is characterized by the absorption chiller. An absorption chiller is a closed loop that uses waste heat to provide cooling or refrigeration. The most widely used absorption working fluids are H_2O-LiBr and NH_3-H_20. Due to critical limitations for the use of the H_2O-LiBr, like the crystallization of the solution or the high vacuum conditions that should be maintained in the system, the NH_3-H_2O solution is used [43]. The H_2O is the refrigerant while the NH_3 is the absorbent. The working principle of the cycle is simply based on different boiling temperatures of the refrigerant and absorbent. A schematic representation of a basic absorption machine is shown in Figure 21 [44].

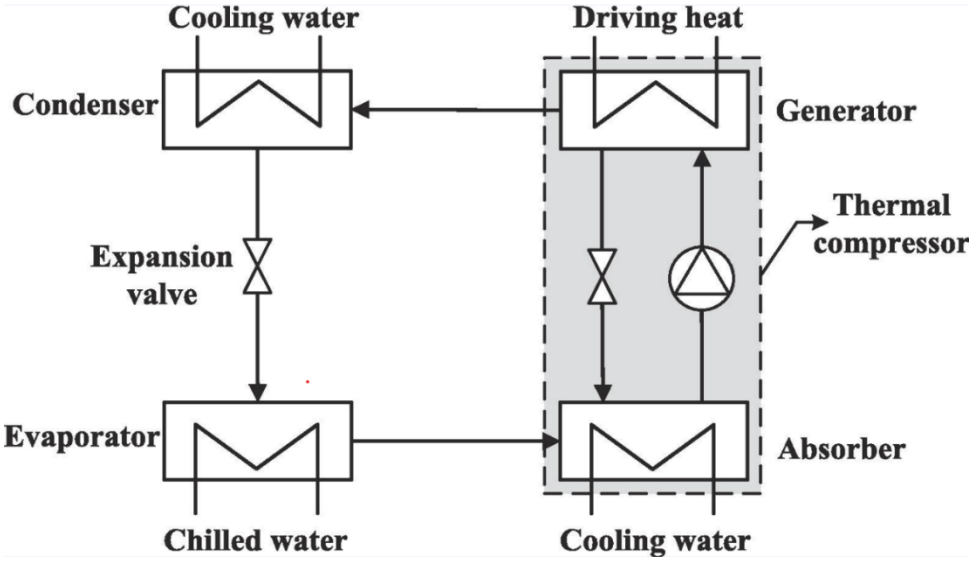

Figure 21. Scheme of a basic absorption chiller

The main components of the cycle are the evaporator, absorber, solution pump, generator, condenser and expansion valves. This cycle works at two pressure levels, the evaporator and the absorber operate in the low-pressure level, while the condenser and the generator operate in the high-pressure one. Firstly, LT heat is transferred from a conditioned space to the evaporator with a chiller water loop to evaporate the refrigerant. Then the refrigerant vapour passes through an absorber where it is absorbed by a concentrated absorbent liquid forming a weak solution. This process releases heat that can be recovered by a cooling water stream. The diluted solution of absorbent and refrigerant is pumped to the generator, where an external heat is provided to boil off the refrigerant from the solution while the concentrated absorbent remains in a liquid form. The liquid rich solution passes through a valve and returns to the absorber while the refrigerant vapour flows to the condenser where heat is rejected to a circulating cooling water loop. The high-pressure liquid refrigerant is expanded with a valve, reducing its pressure and temperature, to be evaporated, closing the cycle.

The position selected for the integration of the absorption chiller cycle in the reference system, in order to overcome the issue related to the H_2O mass flow rate required in the discharge part of the cycle and to exploit the optimum properties of NH_3, is the one located on the condenser of the discharge cycle. In this way the condenser for the discharge cycle is the evaporator for the absorption chiller cycle.

11.2.2.1 Aspen Hysys® modelling

In Figure 22 is reported the scheme of the closed charge and discharge cycles with the integration of the absorption chiller with all the components and the streams. The charge cycle is located at the left of the scheme while the discharge cycle on the right.

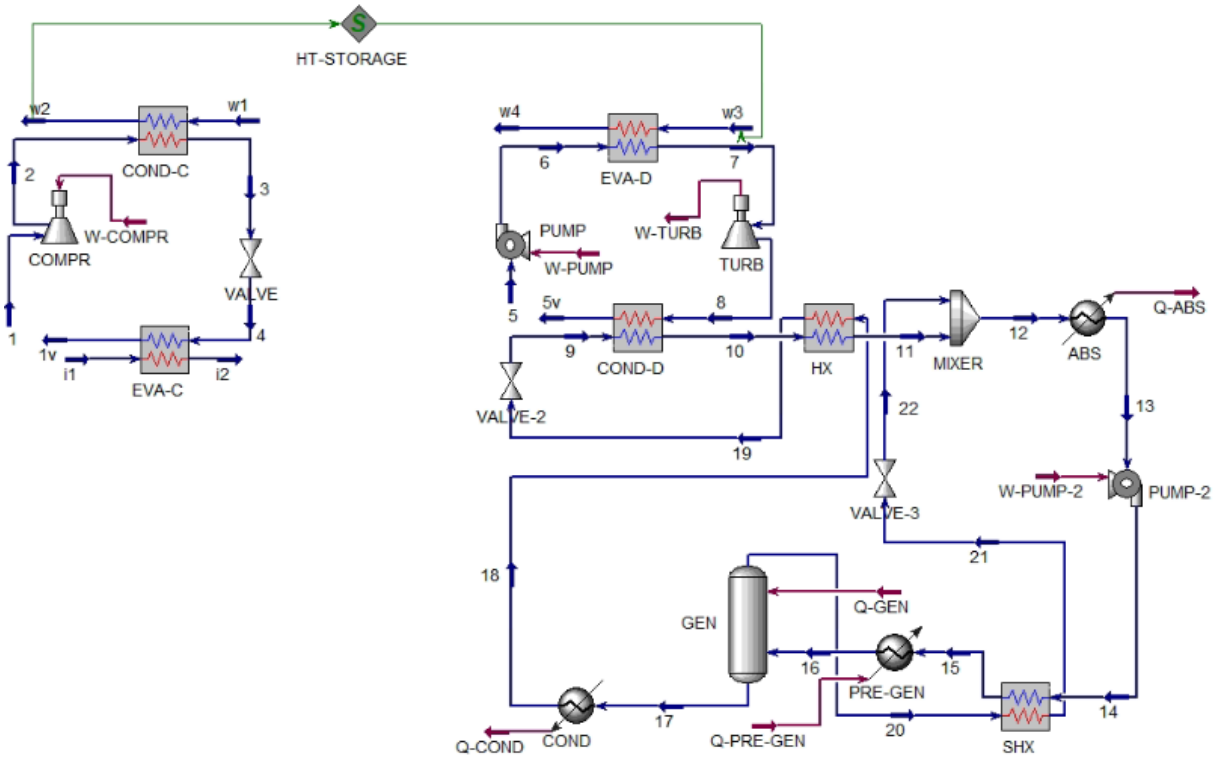

Figure 22. Scheme of the closed cycle paired with the absorption chiller cycle on the discharge part

The components of the charge and discharge cycles are the same of the reference system and their role inside the whole plant remains unchanged.

The absorption chiller cycle is composed of the following components:

- *COND-D - Evaporator:* it condenses the CO_2 on hot side and it evaporates the refrigerant on the cold side.
- *HX - Heat Exchanger:* it increases the temperature of the vapour refrigerant on the cold side and it decreases the temperature of the liquid refrigerant on the hot side.
- *MIXER - Mixer:* it mixes the vapour refrigerant and the liquid rich solution obtaining a weak solution.

- *ABS - Absorber:* it condenses the weak solution before entering the pump.
- *PUMP-2 - Pump:* it increases the pressure and the temperature up to the high-pressure level of the absorption chiller cycle of the weak liquid solution.
- *SHX - Solution Heat Exchanger:* it increases the temperature of the liquid weak solution on the cold side and it decreases the temperature of the liquid rich solution on the hot side.
- *VALVE-3 - Valve:* it expands the liquid rich solution.
- *PRE-GEN - Pre-Generator:* it increases the temperature of the liquid weak solution before entering the generator.
- *GEN - Generator:* it separates the vapour refrigerant from the liquid rich solution.
- *COND - Condenser:* it condenses the vapour refrigerant before entering the heat exchange on the hot side.
- *VALVE-2 - Valve:* it expands the liquid refrigerant up to the low-pressure level of the absorption chiller cycle.

The assumptions and hypothesis made for the closed charge and discharge cycle are the same as the ones reported in Tables 4 and 5. The differences are characterized by the pump input power of the discharge cycle that is reduced to 700 kW and by the elimination of the input condition regarding the minimum approach temperature for the condenser of the discharge cycle. If the same change for the pump power is made for the reference system, the H_2O mass flow rate needed in the condenser of the discharge cycle remains a non-acceptable value equal to 671,8 kg/s.

The system is constructed adding all the components explained above and inserting the input parameters that are summarized in Table 44. [45][46].

Table 43. Main assumptions, inputs and hypothesis on the modelling of the absorption chiller cycle

Input parameters absorption chiller cycle

COND-D	Inlet Temperature Cold Side	-10	°C
HX	Pressure Drop	0	bar
	Outlet Temperature Hot Side	20	°C
ABS	Outlet Vapor Fraction	0	-
PUMP-2	Inlet Mass Flow Rate	30	kg/s
	Outlet Pressure	15	bar
	NH_3 Inlet Volume Fraction	0,5	-
SHX	Minimum Approach Temperature	4	°C
VALVE-3	Outlet Pressure	4	bar
PRE-GEN	Outlet Temperature	110	°C
GEN	Inlet Heat Flux	100	kW
COND	Outlet Vapour Fraction	0	-

The thermodynamic state at each point is obtained and the main output parameters are reported in Table 45. The results for the charge and discharge cycle are equal to the one of the reference system, reported in Table 6, except for CO_2 mass flow rate of the discharge cycle that, due to the decrease for the input value of the pump power, decreases to 35,53 kg/s.

Table 44. Thermodynamic state of the mass streams for the absorption chiller cycle

Stream	*m [kg/s]*	*T [°C]*	*p [bar]*	*Vapour Fraction [-]*	*NH_3 Volume Fraction [-]*
9	8,154	-10	2,645	0,11	0,93
10	8,154	-14,97	2,645	0,87	0,93
11	8,154	32,29	2,645	0,90	0,93
12	30	36,57	2,645	0,22	0,5
13	30	17,98	2,645	0	0,5
14	30	18,10	15	0	0,5
15	30	79,81	15	0	0,5
16	30	110	15	0,28	0,5
17	8,154	110,2	15	1	0,93
18	8,154	41,67	15	0	0,93
19	8,154	20	15	0	0,93
20	21,85	110,2	15	0	0,33
21	21,85	22,07	15	0	0,33
22	21,85	22,32	4	0	0,33

Due to the decrease of the mass flow rate in the discharge cycle the electrical power produced by the turbine decreases as well, as it is equal to 2,477 MW, but the mass flow rate of the refrigerant needed in the condenser of the discharge cycle is an acceptable value, equal to 8,154 kg/s. In Figure 23 is reported the plot that shows the temperatures of hot and cold composites as function of the heat flux exchanged for the discharge cycle. As shown, the refrigerant undergoes a partial phase change from mostly liquid to mostly vapour in the condenser and it performs latent heat exchange.

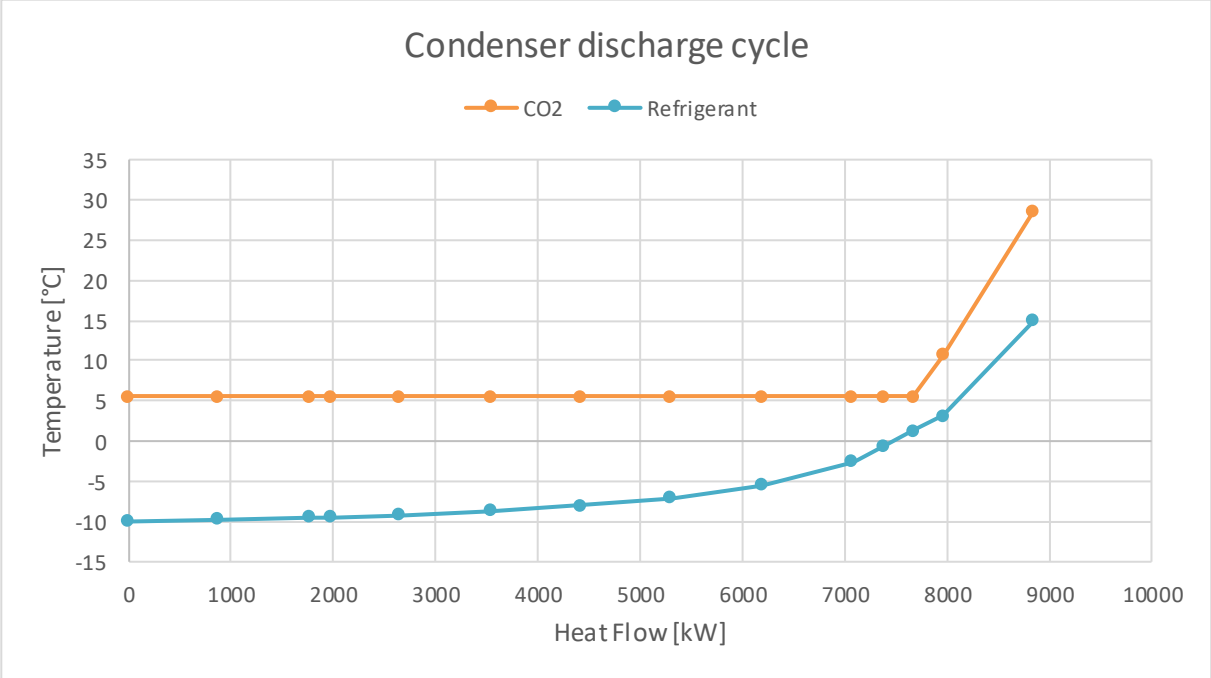

Figure 23. Trend of temperatures as function of heat flow for the condenser of the discharge cycle

11.3 High temperature integration

For the analysed closed system high temperature H_2O is used to perform a sensible heat exchange in the higher part of the charge and discharge cycle.

In order to maximize the power extracted by the turbine and so the performance of the whole system a possible solution can be characterized by the increase of the turbine inlet temperature (TIT) by increasing the temperature of the HT storage. The proposed configuration has this specific purpose using a transcritical closed cycle over the charge part of the reference system.

11.3.1 Cascade heat pump

A cascade heat pump configuration, with a transcritical bottom cycle and a transcritical top cycle can be applied where the gas cooler of the bottom cycle provides superheat to the suction gas in the top cycle. This new cascade arrangement could significantly superheat the suction gas, which will reduce the compression required to reach the same discharge temperature. [47]. The selection of the optimal combination of refrigerants and operating parameters for the two parts of the cycle is non-trivial and a valuable area of research. The scheme of the cascade heat pump configuration modelled is reported in Figure 24.

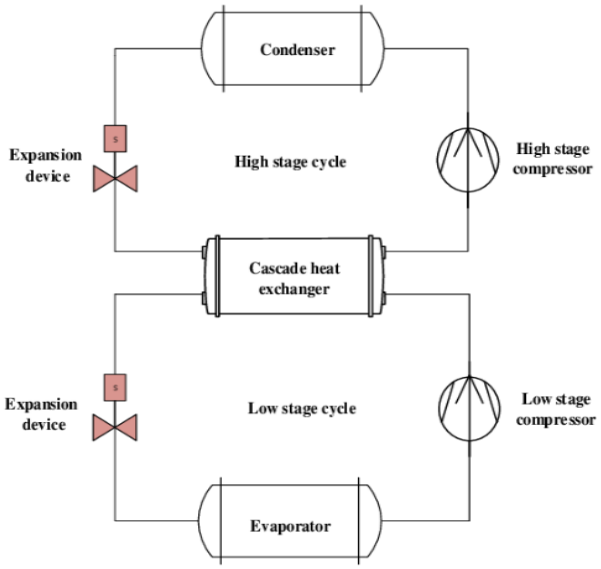

Figure 24. Scheme of cascade transcritical, single-stage (top) and transcritical, single-stage (bottom)

The expected trends for the pressure as function of the enthalpy and for the temperature as function of entropy are reported in Figure 25.

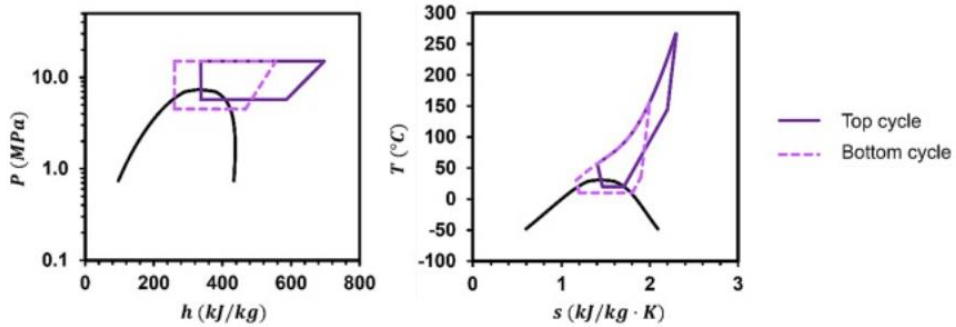

Figure 25. Expected trends for the configuration reported in Figure 24

As it is shown the high-pressure level for both the top and the bottom cycle is the same while the low-pressure level for the bottom cycle is lower comparing to the top one.

11.3.1.1 Aspen Hysys® modelling

In Figure 26 is reported the scheme of the closed charge cycle with the integration of the cascade heat pump and of the closed discharge cycle with all the components and the streams. The charge cycle is located at the left of the scheme while the discharge cycle on the right.

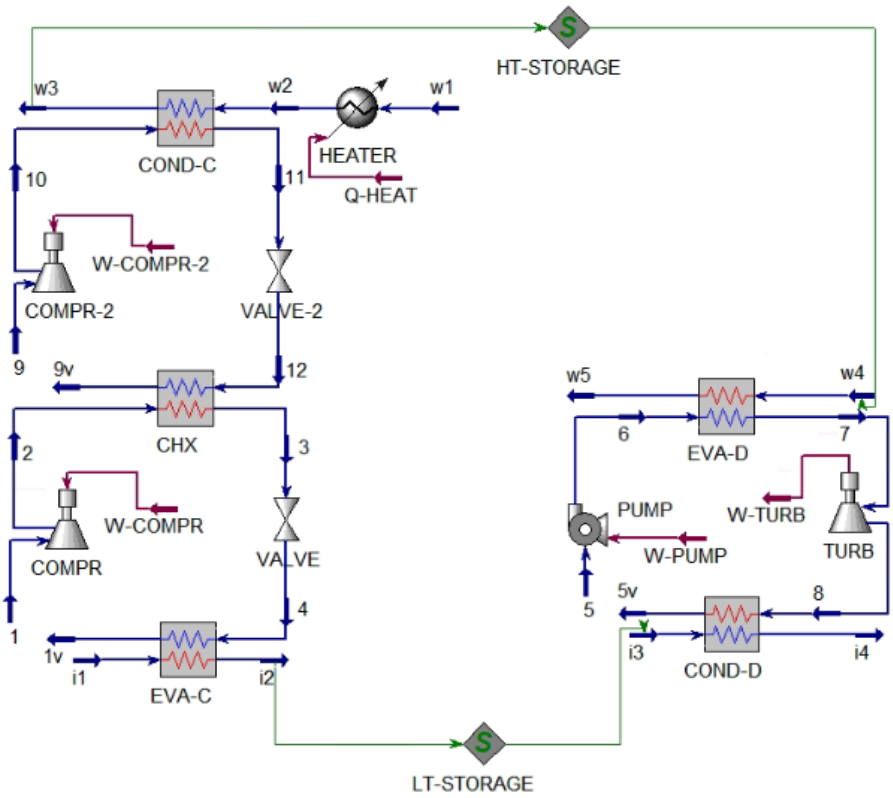

Figure 26. Scheme of the close cycle paired with cascade heat pump on the charge part

The components of the discharge cycle are the same of the reference system and their role remains unchanged. The components of the top and the bottom transcritical charge cycle are the same of the charge cycle of the reference system except for the heater. It is added before the condenser of the top cycle and it uses LT heat to increase the temperature of H_2O before entering the cold side of the heat exchanger. In this way the input parameters are the same of

ones of the reference system, reported in Table 4 and 5, except for the bottom compressor power reduced to 500 kW. Also, the top compressor power is fixed to 500 kW in order to keep the total power required by the charge part of the system equal to the one of the reference system.

The input parameters for the top charge cycle are reported in Table 46.

Table 45. Main assumptions, inputs and hypothesis on the modelling of the cascade heat pump

Input parameters top charge cycle

COMPR-2	Isentropic Efficiency	0,86	-
	Inlet Temperature	161	°C
	Inlet Pressure	50	bar
	Power	500	kW
	Outlet Pressure	200	bar
COND-C	Min Approach Temperature	4	°C
	Pressure Drop	0	bar
	Outlet Vapor fraction Cold Side	0	-
HEATER	Inlet Temperature	30	°C
	Inlet Pressure	12	bar
CHX	Min Approach Temperature	4	°C
	Pressure Drop	0	bar
	Outlet Temperature Hot Side	70	°C
	Inlet Pressure Hot Side	200	bar

The thermodynamic state at each point is obtained and the main output parameters are reported in Table 47.

Table 46. Thermodynamic state of the mass streams for the system with the cascade heat pump

Stream	*m [kg/s]*	*T [°C]*	*p [bar]*	*Vapour Fraction [-]*
1	4,763	-5,048	30	1
2	4,763	165	200	1
3	4,763	70	200	0
4	4,763	-5,046	30	0,66
w1	2,488	30	12	0
w2	2,488	62,56	12	0
w3	2,488	188,1	12	0
i1	8,510	10	5	0
i2	8,510	-1,046	5	0
5	50,75	5,594	40	0
6	50,75	22,66	190	0
7	50,75	184,2	190	1
8	50,75	52,62	40	1
w4	24,38	188,2	12	0
w5	24,38	30	12	0
i3	959,8	-1,046	5	0
i4	959,8	2,355	5	0
9	3,447	161	50	1
10	3,447	322,2	200	1
11	3,447	66,56	200	0
12	3,447	14,40	50	0,56

As expected, due to the reduction of the compressor power in the bottom transcritical cycle also the CO_2 and H_2O mass flow rates for the charge part of the system are reduced to 4,763 kg/s and 2,488 kg/s. The H_2O mass flow rate needed in the condenser of the discharge cycle remains unchanged comparing to the reference system and so equal to 959,8 kg/s.

Moreover, the temperature of the HT storage is increased to 188,1 °C and consequently the electrical power produced by the turbine is increased to 4,095 MW, comparing to the reference system.

12. Conclusions

Large-scale electrothermal energy storage, utilizing transcritical CO_2 cycles and heat transfer to HT and LT H_2O reservoirs is a technology that is still at early stage. The modelling of the reference system analysed in this thesis has highlighted several issues like the imponent amount of heat required in the LT part of the discharge cycle and the consequent imponent H_2O mass flow rate needed as refrigerant. Moreover, the imbalance between the LT and HT tanks, which varies based on the relative size of the storage system and the integrated facility, represents another critical point. In fact, over time, depending on the system size, operating conditions, and level of integration, the LT tank may become fully discharged while the HT tank reaches its maximum capacity, limiting further energy storage. To maintain balance in the tank levels throughout operation, the system needs additional energy input.

The exergo economic analysis of the reference system, performed for the years 2022 and 2023, underlines the actual economic feasibility of this kind of technology. When the electricity cost is high, due to anormal conditions, the system reaches a positive NPV in the estimated lifetime of the plant, but when the electricity cost has a value coherent with the average of the last years, the system never reaches a positive NPV in the estimated lifetime of the plant. It is evident that this technology, without any subsides or incentives, cannot compete with the common ones to produce electrical energy. Further research is necessary to understand how to increase the performance of this plant decreasing the CAPEX and the OPEX.

Different integration scenarios are considered to increase the performance of the system and to solve the issue related to the imponent amount of H_2O mass flow rate required in the LT part of the discharge cycle. The open cycle represents an alternative configuration based on [2] but does not achieve any of the purposes explained above. The LT scenarios presented, instead, manage to decrease the mass flow rate needed by the condenser of the discharge cycle changing the kind of refrigerant. In particular the one using NH_3 is the most efficient one and so an integration scenario based on an absorption chiller cycle that uses NH_3-H_2O solution is proposed. Lastly, an HT scenario based on a cascade heat pump configuration is proposed to increase the performance of the reference system.

13. References

[1] R. Gross, M. Leach, and A. Bauen, "Progress in renewable energy," *Environ Int*, vol. 29, no. 1, pp. 105–122, Apr. 2003, doi: 10.1016/S0160-4120(02)00130-7.

[2] A. Carro, R. Chacartegui, C. Ortiz, J. Carneiro, and J. A. Becerra, "Integration of energy storage systems based on transcritical CO2: Concept of CO2 based electrothermal energy and geological storage," *Energy*, vol. 238, p. 121665, Jan. 2022, doi: 10.1016/j.energy.2021.121665.

[3] A. Mabrouk, J. Labidi, A. Rekik, and M.-R. Jeday, "Exergoeconomic Analysis," 2018, pp. 895–904. doi: 10.1007/978-3-319-62572-0_57.

[4] F. R. McLarnon and E. J. Cairns, "Energy Storage," *Annual Review of Energy*, vol. 14, no. 1, pp. 241–271, Nov. 1989, doi: 10.1146/annurev.eg.14.110189.001325.

[5] S. Tetteh, M. R. Yazdani, and A. Santasalo-Aarnio, "Cost-effective Electro-Thermal Energy Storage to balance small scale renewable energy systems," *J Energy Storage*, vol. 41, p. 102829, Sep. 2021, doi: 10.1016/j.est.2021.102829.

[6] S. Ould Amrouche, D. Rekioua, T. Rekioua, and S. Bacha, "Overview of energy storage in renewable energy systems," *Int J Hydrogen Energy*, vol. 41, no. 45, pp. 20914–20927, Dec. 2016, doi: 10.1016/j.ijhydene.2016.06.243.

[7] C. A. Hendriks and K. Blok, "Underground storage of carbon dioxide," *Energy Convers Manag*, vol. 36, no. 6–9, pp. 539–542, Jun. 1995, doi: 10.1016/0196-8904(95)00062-I.

[8] M. Astolfi, "Technical options for Organic Rankine Cycle systems," in *Organic Rankine Cycle (ORC) Power Systems*, Elsevier, 2017, pp. 67–89. doi: 10.1016/B978-0-08-100510-1.00003-X.

[9] E. G. Feher, "The supercritical thermodynamic power cycle," *Energy Conversion*, vol. 8, no. 2, pp. 85–90, Sep. 1968, doi: 10.1016/0013-7480(68)90105-8.

[10] Y. Ma, Z. Liu, and H. Tian, "A review of transcritical carbon dioxide heat pump and refrigeration cycles," *Energy*, vol. 55, pp. 156–172, Jun. 2013, doi: 10.1016/j.energy.2013.03.030.

[11] B. Yu, J. Yang, D. Wang, J. Shi, and J. Chen, "An updated review of recent advances on modified technologies in transcritical CO2 refrigeration cycle," *Energy*, vol. 189, p. 116147, Dec. 2019, doi: 10.1016/j.energy.2019.116147.

[12] Paul Hawken, *Drawdown: the most comprehensive plan ever proposed to reverse global warming*. New York, 2017.

[13] M. Mercangöz, J. Hemrle, L. Kaufmann, A. Z'Graggen, and C. Ohler, "Electrothermal energy storage with transcritical CO 2 cycles," *Energy*, vol. 45, no. 1, pp. 407–415, Sep. 2012, doi: 10.1016/j.energy.2012.03.013.

[14] P. Nikolai, B. Rabiyat, A. Aslan, and A. Ilmutdin, "Supercritical CO2: Properties and Technological Applications - A Review," *Journal of Thermal Science*, vol. 28, no. 3, pp. 394–430, Jun. 2019, doi: 10.1007/s11630-019-1118-4.

[15] T. Kitto, C. Bodart-Le Guen, N. Rossetti, and F. Cicoira, “Processing and patterning of conducting polymers for flexible, stretchable, and biomedical electronics,” in *Handbook of Organic Materials for Electronic and Photonic Devices*, Elsevier, 2019, pp. 817–842. doi: 10.1016/B978-0-08-102284-9.00025-5.

[16] T. Neises and C. Turchi, “A Comparison of Supercritical Carbon Dioxide Power Cycle Configurations with an Emphasis on CSP Applications,” *Energy Procedia*, vol. 49, pp. 1187–1196, 2014, doi: 10.1016/j.egypro.2014.03.128.

[17] A. Hepbasli and Y. Kalinci, “A review of heat pump water heating systems,” *Renewable and Sustainable Energy Reviews*, vol. 13, no. 6–7, pp. 1211–1229, Aug. 2009, doi: 10.1016/j.rser.2008.08.002.

[18] H. G. Siewert, “Compressor Tolerance to Liquid Refrigerant,” in *International Compressor Enginerring Conference*, School of Mechanical Engineering, 1972, pp. 1–6. [Online]. Available: https://docs.lib.purdue.edu/icec

[19] J. Straus and S. Skogestad, “Minimizing the complexity of surrogate models for optimization,” *Computer Aided Chemical Engineering*, vol. 38, pp. 289–294, Jan. 2016, doi: 10.1016/B978-0-444-63428-3.50053-9.

[20] A. Technology, “Aspen Physical Property Methods,” 2013. [Online]. Available: http://www.aspentech.com

[21] J. M. P. Sala Lizarraga and A. Picallo-Perez, “Calculation of physical and chemical exergy,” *Exergy Analysis and Thermoeconomics of Buildings*, pp. 183–259, Jan. 2020, doi: 10.1016/B978-0-12-817611-5.00003-5.

[22] Bhavik R. Bakshi, Timothy G. Gutowski, and Dušan P. Sekulić, “Appendix: Standard Chemical Exergy,” in *Thermodynamics and the Destruction of Resources*, Cambridge University Press, 2011, pp. 489–494. doi: 10.1017/CBO9780511976049.024.

[23] Harry. Silla, *Chemical process engineering : design and economics*. M. Dekker, 2003.

[24] Adrian Bejan, George Tsatsaronis, and Michael Moran, *Thermal Design and Optimization*. New York: Wiley-Interscience, 1996.

[25] Charles Maxwell, “https://toweringskills.com/financial-analysis/cost-indices/.”

[26] K. Lu, I. A. Sultan, and T. H. Phung, “A Literature Review of the Positive Displacement Compressor: Current Challenges and Future Opportunities,” *Energies (Basel)*, vol. 16, no. 20, p. 7035, Oct. 2023, doi: 10.3390/en16207035.

[27] Heinz P. Bloch, “A Practical Guide to Compressor Technlogy,” 2006.

[28] M. E. Qazizada, V. Sviatskii, and P. Bozek, “Analysis performance characteristics of centrifugal pumps,” *MM Science Journal*, vol. 2016, no. OCTOBER, pp. 1151–1159, Oct. 2016, doi: 10.17973/MMSJ.2016_10_201691.

[29] R. K. Shah and D. P. Sekulic, *Fundamentals of Heat Exchanger Design*. New York: Wiley-Interscience, 2003.

[30] J. Theis, “Quality Guidelines for Energy Systems Studies: Cost Estimation Methodology for NETL Assessments of Power Plant Performance - Feb 2021,” Feb. 2021. doi: 10.2172/1567736.

[31] “http://www.market-risk-premia.com/es.html.”

[32] Banco de España, “https://clientebancario.bde.es/pcb/en/menu-horizontal/productosservici/relacionados/tiposinteres/guia-textual/tiposinteresrefe/tabla_tipos_compensacion_riesgo_tipo_interes.html?anyo=f7bdea007227e710VgnVCM10000083f614acRCRD.”

[33] Aswath Damodaran, “https://pages.stern.nyu.edu/~adamodar/New_Home_Page/datafile/ctryprem.html.”

[34] J. Yuan, C. Cui, Z. Xiao, C. Zhang, and W. Gang, “Performance analysis of thermal energy storage in distributed energy system under different load profiles,” *Energy Convers Manag*, vol. 208, p. 112596, Mar. 2020, doi: 10.1016/j.enconman.2020.112596.

[35] “https://tarifaluzhora.es/info/precio-kwh/evolucion-precio-luz.”

[36] T. Wilberforce, A. G. Olabi, E. T. Sayed, K. Elsaid, and M. A. Abdelkareem, “Progress in carbon capture technologies,” *Science of The Total Environment*, vol. 761, p. 143203, Mar. 2021, doi: 10.1016/j.scitotenv.2020.143203.

[37] R. Svensson, M. Odenberger, F. Johnsson, and L. Strömberg, “Transportation systems for CO2—application to carbon capture and storage,” *Energy Convers Manag*, vol. 45, no. 15–16, pp. 2343–2353, Sep. 2004, doi: 10.1016/j.enconman.2003.11.022.

[38] J. Gale, “Geological storage of CO2: What do we know, where are the gaps and what more needs to be done?,” *Energy*, vol. 29, no. 9–10, pp. 1329–1338, Jul. 2004, doi: 10.1016/j.energy.2004.03.068.

[39] A. Carro, R. Chacartegui, C. Ortiz, J. Carneiro, and J. A. Becerra, “Energy storage system based on transcritical CO2 cycles and geological storage,” *Appl Therm Eng*, vol. 193, p. 116813, Jul. 2021, doi: 10.1016/j.applthermaleng.2021.116813.

[40] A. K. Vuppaladadiyam *et al.*, “Progress in the development and use of refrigerants and unintended environmental consequences,” *Science of The Total Environment*, vol. 823, p. 153670, Jun. 2022, doi: 10.1016/j.scitotenv.2022.153670.

[41] M. Sruthi Emani, R. Roy, and B. Kumar Mandal, “DEVELOPMENT OF REFRIGERANTS: A BRIEF REVIEW,” *Indian J.Sci.Res*, vol. 14, no. 2, pp. 175–181, 2017.

[42] D. Calleja-Anta, L. Nebot-Andrés, J. Catalán-Gil, D. Sánchez, R. Cabello, and R. Llopis, “Thermodynamic screening of alternative refrigerants for R290 and R600a,” *Results in Engineering*, vol. 5, p. 100081, Mar. 2020, doi: 10.1016/j.rineng.2019.100081.

[43] W. Wu, B. Wang, W. Shi, and X. Li, “An overview of ammonia-based absorption chillers and heat pumps,” *Renewable and Sustainable Energy Reviews*, vol. 31, pp. 681–707, Mar. 2014, doi: 10.1016/j.rser.2013.12.021.

[44] A. Shirazi, R. A. Taylor, G. L. Morrison, and S. D. White, “Solar-powered absorption chillers: A comprehensive and critical review,” *Energy Convers Manag*, vol. 171, pp. 59–81, Sep. 2018, doi: 10.1016/j.enconman.2018.05.091.

[45] C. Somers, A. Mortazavi, Y. Hwang, R. Radermacher, S. Al-Hashimi, and P. Rodgers, “Modeling Absorption Chillers in ASPEN,” Abu Dhabi, Nov. 2008.

[46] R. Mansouri, I. Boukholda, M. Bourouis, and A. Bellagi, “Modelling and testing the performance of a commercial ammonia/water absorption chiller using Aspen-Plus platform,” *Energy*, vol. 93, no. Part 2, pp. 2374–2383, Dec. 2015, doi: 10.1016/J.ENERGY.2015.10.081.

[47] K.-M. Adamson *et al.*, “High-temperature and transcritical heat pump cycles and advancements: A review,” *Renewable and Sustainable Energy Reviews*, vol. 167, p. 112798, Oct. 2022, doi: 10.1016/j.rser.2022.112798.

Ringraziamenti

Ho faticato molto a scrivere questi ringraziamenti, molto di più di quanto non abbia fatto per quelli della triennale e ho rimandato fino all'ultimo minuto quest'onere. Cercavo un'illuminazione, una frase ad effetto con cui cominciare, un artificio che lasciasse senza parole chi li avesse letti. Ma i ringraziamenti sono solo ringraziamenti e quello che è scritto qui, in realtà l'ho già detto (attraverso le azioni, visto le mie scarse capacità dialettiche) ai diretti interessati.

Thank to my supervisor Ricardo for all your support, endless help and understanding that you have shown in every step of this thesis, probably without them I'd still write page 1.

Grazie nonna Tetta, per aver avuto fiducia in me e nel mio percorso in ogni momento più di quanto non l'abbia mai avuta io. Grazie per avermi spronata a credere di più in me stessa e per aver condiviso la tua storia ed i tuoi ricordi ampliando il mio modo di vedere il mondo.

Grazie nonna Giovanna, per avermi ospitato sempre quando volevo tornare dalle mie montagne, per aver condiviso pettegolezzi e risate di fronte ad un bicchiere di prosecco.

Grazie mamma, per l'infinito sostegno che mi hai dato in questi anni, grazie per aver capito i miei stati d'animo ed averli assecondati, per avermi insegnato a vivere con saggezza e coraggio. Grazie per non aver interferito in nessuna delle mie scelte e per esserti sforzata di comprenderle e grazie per l'affetto che mi hai sempre dimostrato in modo incondizionato.

Grazie papà, per la calma e l'energia che mi hai trasmesso in questi anni, mi hanno aiutato a fermarmi e riflettere in questo turbine che è stata la mia vita ultimamente. Grazie per i silenzi condivisi nelle passeggiate in montagna e per i pipponi sul Tai Chi, grazie per avermi sempre accolto in Valtellina con più o meno lo stesso entusiasmo di quando Bruce mi salta addosso e mi morde la faccia.

Grazie Antonella, per l'ascolto e il supporto che mi hai fornito nella mia vita universitaria e non. Grazie per l'infinta pazienza che hai sempre dimostrato nei miei confronti, grazie per essere entrata nella mia vita per portare solo più luce.

Grazie Sofi, per essere l'incredibile persona che sei, per aver ascoltato le mie confidenze e per avermi consigliata sempre con saggezza. Grazie per esserci stata quando ne avevo bisogno o anche solo quando cercavo compagnia per bere un vinello. Sono così fiera di te e del percorso che hai fatto in questi anni, grazie per aver lasciato che ne facessi parte.

Grazie Ari, per avermi aiutato a comprendermi meglio, soprattutto le parti di me che mi piacciono di meno e per essermi stata vicino in molti momenti di questi ultimi anni. Nonostante in questo momento siamo con le pezze ar culo, per usare un francesismo, so che faremo sempre parte della vita dell'altra e confido nel fatto che, quando servirà, saremo in grado di fare un passo indietro per essere gentili.

Grazie Gio, tu più di tutti sei stata il grigri che ha bloccato la corda quando stavo cadendo faccia a terra. So che continueremo a condividere le nostre vite con leggerezza e risate, con prese in giro ed improvvisazione, con pianti e birrette incastrando le nostre asperità come parte dell'opera d'arte che è la nostra amicizia. Grazie per il tempo che mi hai dedicato quando ne ho avuto bisogno, non l'ho mai dato per scontato.

Grazie Sara, per aver condiviso con me cammini ed arrampicate, serate a bere e a fumare e giornate al parco, tendate e pasti vegetariani. Sei un piccolo caleidoscopio sempre in movimento e confido che nel nostro fluire troveremo rocce che ci permetteranno di fermarci ed ascoltarci a vicenda, cosa che credo fino ad ora abbiamo fatto.

Grazie Giorgia, sei entrata nella mia vita in un momento incredibilmente delicato e in poco tempo sei diventata una delle ghiere a cui affiderei le mie calate. Grazie per l'ascolto e il supporto che mi hai fornito in questo anno e mezzo, per le pizze in compagnia ordinate in tarda serata in aula studio e per le bottiglie di vinello accompagnate da pettegolezzi e confidenze. Grazie per esserci stata sempre, nelle giornate serene e in quelle burrascose.

Grazie Marti, per essere il mio punto fermo ogni volta che scendo a Tivoli riuscendo a rendere i miei rientri in patria decisamente più divertenti. Grazie perché, da quando ti conosco, mi forzi a vedere il mondo in un modo che non mi appartiene ma che apprezzo e stimo.

Grazie Chiara, per le "produttive" giornate di studio e per gli aperitivi improvvisati, per l'incredibile leggerezza che hai portato nella mia vita in questa città.

Grazie Maggio, per aver condiviso parte di questi ultimi anni con me. Grazie perché mi hai insegnato a lasciar cadere le difese che avevo eretto negli anni, mi hai aiutato a ritrovarmi e mi hai ascoltato davvero, dando sempre peso alle mie parole. Ci siamo fatti del bene e del male, ma sono convinta che alla fine tutto ha avuto un senso, tutto faceva parte di un disegno che non riesco a vedere adesso ma che spero in futuro di riuscire ad apprezzare nella sua interezza.

Grazie Enrico, la tua presenza nella mia vita sivigliana l'ha arricchita e resa incredibilmente più divertente. Grazie per essermi stato vicino ed avermi ascoltato quando volevo condividere, grazie per non avermi mai fatto sentire sbagliata o eccessivamente fricchettona.

Thank to Robert, Chris and Kim, you brought meaning to my life in Sevilla, joining pieces of myself that were fluttering away. I have faith that our paths will cross again maybe in a different time and space. Thank for all the laughs and cervezas that we have shared together.

Grazie a tutti gli amici che hanno fatto parte del mio percorso universitario, grazie per le risate, per le serate a chiacchierare e per quelle a bere. Siete stati una grande parentesi serena di questi ultimi anni grazie alla quale sono riuscita a sentirmi a casa in una città che ho sempre fatto fatica a considerare casa mia.

Grazie a tutti gli amici arrampicatori che ho, o non ho, conosciuto al Bside. Grazie per avermi contagiato con la vostra energia positiva ed avermi offerto una facile via di fuga da questa città, senza necessariamente dover scappare dall'altra parte del mondo. Grazie per aver reso la mia routine più simile a come l'ho sempre voluta.

Grazie a tutti i ragazzi di Santiago, in qualche modo so che sarete sempre presenti nella mia vita quando avrò bisogno di sostegno o di svuotare la mente camminando. Ognuno di voi mi ha dato tanto e mi ha aiutato a vedere il mondo da una prospettiva diversa. Grazie.

Grazie a tutte le persone che non sono finite in questi ringraziamenti ma che comunque hanno fatto parte della mia vita, anche solo per dieci minuti di attesa per la farinata. Grazie per avermi offerto spunti di riflessione, sorrisi, abbracci, conforto, serate divertenti e spensierate.

Grazie perché nel grande casino che è la mia vita, come quella di tutti, l'unica cosa che davvero conta sono le persone che hanno fatto parte del mio percorso e quello che siamo riuscite a darci a vicenda, un piccolo spiraglio di luce laddove non si riusciva a vederlo da soli.